Chromokinesin KIF4A teams up with Stathmin 1 to regulate abscission in a SUMO-dependent manner

Sabine A.G. Cuijpers[1,3], Edwin Willemstein[1], Jan G. Ruppert[2,4], Daphne M. van Elsland[1], William C. Earnshaw[2] and Alfred C.O. Vertegaal[1*]

[1] Cell and Chemical Biology, Leiden University Medical Center, 2333 ZA Leiden, the Netherlands

[2]Wellcome Centre for Cell Biology, University of Edinburgh, EH9 3JR Edinburgh, Scotland, UK

[3]present address: AbSano B.V., Oss, the Netherlands

[4]present address: Boehringer Ingleheim, Mainz, Germany

* Corresponding author: Alfred C. O. Vertegaal, e-mail: vertegaal@lumc.nl

Keywords: mitosis; abscission; cytokinesis; KIF4A; post-translational modification; SUMO; Stathmin 1

JCS Advance Online Article. Posted on 26 June 2020

Summary statement

A new mechanism of abscission regulation is identified through the dynamic interactions between KIF4A and Stathmin 1 as controlled by SUMO modification of KIF4A.

Abstract

Cell division ends when two daughter cells physically separate via abscission, the cleavage of the intercellular bridge. It is not clear how the anti-parallel microtubule bundles bridging daughter cells are severed. Here, we present a novel abscission mechanism. We identified the chromokinesin KIF4A adjacent to the midbody during cytokinesis which is required for efficient abscission. KIF4A is regulated by post-translational modifications. We evaluated modification of KIF4A by the ubiquitin-like protein SUMO. We mapped lysine 460 in KIF4A as the SUMO acceptor site and employed CRISPR-Cas9 mediated genome editing to block SUMO conjugation of endogenous KIF4A. Failure to SUMOylate this site in KIF4A delayed cytokinesis. SUMOylation of KIF4A enhances affinity for the microtubule destabilizer Stathmin1. We here present a new level of abscission regulation through the dynamic interactions between KIF4A and Stathmin 1 as controlled by SUMO modification of KIF4A.

Introduction

Abscission is the last step of cell division in which the two daughter cells are finally separated to start their own independent life. Our present understanding of abscission is limited (Mierzwa and Gerlich, 2014). Prior to abscission, the cleavage furrow is formed involving key players like actin, myosin, septin and anillin culminating in the constricted intercellular bridge (Field and Alberts, 1995; Joo et al., 2007; Lewellyn et al., 2011; Mabuchi, 1994; Mavrakis et al., 2014; Mullins and Biesele, 1977; Nunnally et al., 1980; Reichl et al., 2008; Sanger et al., 1994; Schroeder, 1968; Uehara et al., 2010; Zhou and Wang, 2008). Subsequently, the cortex of the intercellular bridge is narrowed to a single stalk of 17-nanometer-diameter filaments (Guizetti et al., 2011). This process involves the ESCRT-III complex and spastin-mediated microtubule disassembly (Connell et al., 2009; Yang et al., 2008). Although spastin knockdown results in a delay in microtubule disassembly, the process is not abolished, indicating the existence of additional abscission pathway components.

Post-translational modifications play a major role in mitotic regulation. Important modifications include phosphorylation and modification by small proteins including ubiquitin and small ubiquitin-like modifier (SUMO) (Barr et al., 2004; Cubenas-Potts et al., 2015; Dasso, 2008; Deribe et al., 2010; Eifler and Vertegaal, 2015; Flotho and Melchior, 2013; Gareau and Lima, 2010; Glotzer et al., 1991; Gurley et al., 1973; King et al., 1994; King et al., 1996; Li and Hochstrasser, 1999; Peters, 2002; Ribet et al., 2017; Pohl and Jentsch, 2008; Seeler and Dejean, 2017; Seufert et al., 1995; Teixeira and Reed, 2013; Zhang et al., 2008). Inactivating SUMO conjugation machinery components indeed delays cell cycle progression and results in chromosomal aberrations (Hayashi et al., 2002; He et al., 2015; Nacerddine et al., 2005; Schimmel et al., 2014), but it is unclear how. SUMO is conjugated to hundreds of substrates (Hendriks et al., 2014; Hendriks and Vertegaal, 2016a; Schimmel et al., 2014), but little is known about the impact of SUMO on key substrates in mitosis. What is observed is that SUMO accumulates at the midbody during cytokinesis, but -again- its functional relevance nor the relevant substrates for cytokinesis are unclear (Fu et al., 2005; Nie and Boddy, 2016; Pelisch

et al., 2017). One protein critical for cytokinesis is the chromokinesin KIF4A that is preferentially localized at the midbody, is important for PRC1 recruitment and for microtubule organization at the midbody (Hu et al., 2011; Kurasawa et al., 2004; Lee and Kim, 2004; Zhu et al., 2005; Zhu et al., 2006). Here, we identified KIF4A as a SUMOylated protein and show that this modification is important for dynamic interaction with the microtubule destabilizer Stathmin1. SUMO thus participates in cytokinesis.

Results

The human chromokinesin KIF4A is modified by one SUMO moiety

We aimed to understand the mechanisms and effects of SUMOylation of the chromokinesin KIF4A (Cubenas-Potts et al., 2015; Kurasawa et al., 2004) to obtain more detailed understanding of how SUMO regulates this important process of mitosis (Fig. 1A). KIF4A has been identified as SUMO target protein in at least ten individual SUMOylation proteomics studies, indicating that this protein is one of the top targets for SUMO (Hendriks et al., 2014; Hendriks and Vertegaal, 2016a; Schimmel et al., 2014). Immunoblot analysis confirmed KIF4A as a SUMO target . To enrich for SUMOylated proteins, U2OS cell lines either or not stably expressing His_{10}-SUMO2 at close to endogenous levels were lysed and a His_{10}-pulldown was performed. Immunoblot analysis revealed modification of endogenous KIF4A by one single SUMO moiety (Fig. 1B). This was confirmed transfecting U2OS cells with either control or HA-KIF4A constructs. After enrichment for KIF4A by HA-IP, under conditions where SUMOylation is preserved, immunoblotting against SUMO2/3 confirmed modification of HA-KIF4A by endogenous SUMO2/3 (Fig. 1C). Additionally, HA-KIF4A enriched in a non-denaturing manner was able to be SUMOylated *in vitro* upon addition of SUMO E1, SUMO E2 and SUMO2 (Fig. 1D).

While KIF4A was quantitatively modified by SUMO under in vitro conditions, this is considerably lower in tissue culture cells as the SUMOylated fraction of KIF4A could not be

observed by staining for bulk KIF4A in input samples. The modification might be specific for a certain cell cycle phase or for a functionally distinct fraction of KIF4A. However, no clear dynamic SUMOylation levels for KIF4A were observed throughout the cell cycle (Fig. S1) or during mitosis (Fig. S2). This suggests that either the time window during which the fraction of SUMOylated KIF4A shows dynamics is too small to resolve using this experimental set-up, or that a specific fraction of SUMOylated KIF4A is continuously present.

KIF4A is SUMOylated on lysine 460 in a SIM dependent manner

Modification by one single SUMO2 moiety indicates targeting of a particular lysine residue in KIF4A. Various lysine-to-arginine KIF4A mutants were made to localize the SUMO acceptor lysine in KIF4A and transfected into U2OS cell lines without or with stable expression of His_{10}-SUMO2. Mutating lysine 460 to arginine (K460R) abolished HA-KIF4A SUMOylation (Fig. 2A). The SUMO E2 UBC9 reportedly recognizes the consensus SUMOylation motif KxE in target proteins (Bernier-Villamor et al., 2002). Although KIF4A lysine 460 is not located in this specific motif, two adjacent glutamic acid residues could be part of either an inverted consensus motif ExK (Matic et al., 2010) or a less common KE motif (Pichler et al., 2005). While the single motif mutations did not abolish HA-KIF4A SUMOylation, replacing both glutamic acid residues simultaneously did, suggesting that both motifs can be utilized by the SUMO conjugation machinery in cells in a redundant manner.

To verify these results, an *in vitro* SUMOylation assay was performed on purified HA-KIF4A wildtype (WT) and mutant proteins. While WT HA-KIF4A was SUMOylated upon addition of SUMO2, both the K460R and E458/461A mutants were not, confirming the results obtained from cells (Fig. 2B). However, unlike our observation in cells, mutating the inverted consensus motif was sufficient to abolish KIF4A SUMOylation *in vitro*. The *in vitro* assay only contains SUMO E1 and SUMO E2. However, cells express various SUMO E3s proteins that can contribute to the specific modification of KIF4A. Yet, our experiments suggest that KIF4A SUMOylation occurs via two complementary mechanisms either through direct recognition of the inverted consensus motif by UBC9 or supported by a SUMO E3 to recognize the KE motif.

Interestingly, in depth analysis of the sequence of KIF4A also revealed a potential SUMO interaction motif (SIM) at aa 148-152, located within the motor domain of this kinesin family member. To determine whether the SIM influences SUMOylation of KIF4A, this motif was separately mutated from ILDLL to AADAA to keep the hydrophobic nature of the amino acids, but to prevent SUMO interaction according to common practice in the SUMO field. U2OS cells either or not stable expressing of His_{10}-SUMO2 were transfected with WT or mutant HA-KIF4A plasmids. Upon His_{10}-pulldown and immunoblot analysis, the SIM mutation was observed to abolish SUMOylation of each of these three HA-KIF4A constructs (Fig. 2C). Thus KIF4A SUMOylation requires this SIM. Therefore, we propose that a SUMO-UBC9 complex is able to bind the SIM in KIF4A, which brings the SUMO E2 in close proximity to lysine 460 to either directly recognize the inverted consensus motif or SUMOylate KIF4A with the help of a SUMO E3 (Fig. 2D).

Does SUMO modification affect the activity of the motor protein KIF4A? We performed an ATPase activity assay to follow KIF4A activity in the absence and presence of modification by SUMO2. Recombinant GST-KIF4A WT or SUMOylation deficient mutants (K460R and E458/461A) were incubated with SUMOylation mix in the absence or presence of SUMO2 to generate KIF4A proteins either or not modified by SUMO2. ATPase activity assays were performed in the absence or presence of microtubules (MTs), since MT binding is required for specific KIF4A ATPase activity as required for motor activity. WT GST-KIF4A was active in the presence of MTs as expected, but SUMOylation did not affect the ATPase activity of KIF4A (Fig. 3A). Aliquots of the samples were analyzed by immunoblotting to confirm *in vitro* SUMOylation (Fig. 3B). This suggests that both KIF4A mutants are functional for MT binding and dimerization, since both are essential for ATPase activity, and SUMO modification is not critical for KIF4A motor activity.

Mutating lysine 460 in endogenous KIF4A via genome editing by CRISPR-Cas9 abolishes SUMOylation

We next studied the role of KIF4A SUMOylation *in vivo* by genetic manipulation in U2OS cells. CRISPR-Cas9-directed genome editing was used in combination with a repair template to mutate the endogenous KIF4A gene to yield the K460R mutant. Each clone was tested by PCR and digestion with restriction enzymes, followed by sequencing of candidates. Finally, three clones were identified for which the corresponding codon AAA encoding lysine 460 was mutated into codon AGA encoding an arginine (Fig. S3). For each KIF4A mutant (K460R) clone, an individual KIF4A control (WT) clone was selected which had undergone exactly the same procedure at the same moment without introducing any mutations. To check SUMOylation of KIF4A, these three WT and three K460R clones were infected with lentivirus encoding His_{10}-SUMO2 and selected by puromycin to obtain stable cell lines. His_{10}-pulldown and immunoblot analysis revealed complete abolishment of KIF4A SUMOylation in all three KIF4A K460R mutant clones, while WT KIF4A in all three control clones was confirmed to be SUMOylated (Fig. 4A).

Since SUMOylation can affect the subcellular localization of target proteins, cells of each clone were plated on glass slides and stained for endogenous KIF4A by immunofluorescence. Co-staining against tubulin and DNA enabled recognition of cells in various stages of mitosis. WT KIF4A was observed to localize primarily at the midzone during anaphase and at the midbody during cytokinesis in all three control clones (Fig. 4B and Fig. S4A). No differences in localization were observed for K460R KIF4A in any of the three mutant clones (Fig. 4C and Fig. S4B). Thus, the subcellular localization of KIF4A is not regulated by SUMOylation at position K460.

SUMOylation of endogenous KIF4A regulates abscission

While studying the samples to determine KIF4A localization during mitosis (Fig. 5A), the relative amount of cells in mitosis caught our attention. Indeed, upon quantification, an increased percentage of mitotic cells was observed for each K460R mutant clone compared

to its WT control clone (Fig. S5A). The results obtained for all three WT cell lines and the results obtained for all three K460R cell lines were averaged (Fig. 5B). To determine whether the increased percentage of cells in mitosis could be attributed to a specific mitotic phase, cells were categorized into prophase/prometaphase, metaphase, anaphase and telophase/cytokinesis. This detailed analysis revealed an increased percentage of cells in telophase/cytokinesis for the K460R clones compared to their corresponding WT clones (Fig. 5C and Fig. S5B), suggesting a role for SUMOylated KIF4A during this final stage of cell division.

To study this phenotype in more detail, the WT and K460R clones were transfected with GFP-tubulin and selected to create stable cell lines (Fig. S5C). Live cell imaging was performed using differential interference contrast (DIC) to visualize the moment of anaphase onset and GFP-tubulin to identify disconnection of the intercellular microtubule bridge at the end of cytokinesis, which was marked as the moment of abscission. Mitotic cells with a K460R KIF4A background needed significantly longer (median of 168 minutes) to proceed from anaphase onset to abscission compared to cells expressing WT KIF4A protein (median of 114 minutes) (Fig. 5D and Fig. S5D). These data indicate that the increased percentage of cells in cytokinesis is the result of an abscission delay, uncovering a SUMO-regulated function for KIF4A in this final step of cell division.

SUMOylation of KIF4A enhances binding to microtubule destabilizer STMN1

SUMOylation of target proteins can affect their binding to other proteins. To determine whether SUMOylation contributes to proper regulation of abscission through affecting binding of KIF4A to specific partners, a mass spectrometry screen was performed (Fig. 6A). Recombinant GST-KIF4A WT and K460R mutant were incubated with SUMOylation mix (Fig. S6A). As an additional negative control SUMO2 was omitted as indicated. Samples were bound to beads and washed, prior to incubation with U2OS cell lysate. After additional washing and sample preparation, peptides were measured by mass spectrometry. Furthermore, aliquots of the protein samples were analyzed by immunoblotting to confirm the presence of (SUMOylated)

KIF4A after incubation with the U2OS cell lysate (Fig. S6B). Sample analysis revealed a significant preference of the microtubule destabilizer Stathmin 1 (STMN1) for SUMOylated WT KIF4A compared to non-SUMOylated WT KIF4A (Fig. 6B). Differential binding of STMN1 was also found by mass spectrometry when comparing SUMOylated WT KIF4A with K460R KIF4A which was incubated with the complete SUMOylation mix (Fig. 6C).

Preferential binding of recombinant GST-STMN1 to SUMOylated KIF4A was subsequently confirmed by immunoblotting (Fig. 6D-E). Whereas STMN1 also binds to non-SUMOylated KIF4A, quantification of three independent experiments confirmed increased binding of STMN1 to SUMOylated KIF4A (Fig. 6F).

Discussion

The function of SUMO, a small ubiquitin-like modifier is considerably worse understood when compared to ubiquitin itself. Here we studied the role of the SUMO modification of KIF4A. We identify an important role of SUMOylated KIF4A in the regulation of abscission as this controls the interaction with the microtubule destabilizer STMN1. This is summarized in a model in Fig. 7. SUMOylation of KIF4A increases its affinity for STMN1. Since KIF4A is a plus-end directed motor protein, enhanced binding of STMN1 to SUMOylated KIF4A could affect the relative concentration of STMN1 along microtubules, possibly enhancing concentration at the plus-end (Nouar et al. 2016). This could lead to local microtubule destabilization to enable timely separation of daughter cells. Interestingly, no phosphorylated peptides of this microtubule destabilizing protein were identified by our mass spectrometry, indicating that SUMOylated KIF4A interacts with the active form of STMN1 (Larsson et al., 1997). In the absence of KIF4A SUMOylation, decreased binding of KIF4A to STMN1 may result in slower microtubule destabilization and subsequently a delay in cytokinesis. Whereas it was previously found that SUMO2/3, KIF4A and STMN1 are all important players in the earlier stages of mitosis, our

new results suggest that these proteins team-up in a dynamic model to regulate cytokinesis, the final step of cell division.

The SUMOylation site and SIM in KIF4A are well conserved amongst higher eukaryotes, but are missing in model lower eukaryotes such as *Drosophila melanogaster* and *Caenorhabditis elegans* (Fig. S7). This corresponds with the absence of STMN1 in these lower eukaryotes. Interestingly, these conservation patterns correlate exactly with the process of open mitosis characteristic for higher eukaryotic cells (Guttinger et al., 2009).

Mechanistically, we report the first *in vitro* SUMOylation via the inverted SUMO consensus motif (Matic et al., 2010) upon addition of only SUMO E1 and SUMO E2, indicating that UBC9 is able to directly recognize and modify the ExK motif. The SIM in KIF4A is essential for its SUMOylation and most likely responsible for the recruitment of the SUMO-charged UBC9 complex either or not employing a SUMO conjugated to UBC9 itself (Pichler et al., 2017).

To gain more insight into the effect of SUMO on KIF4A function, we have employed CRISPR-Cas9 genome editing and obtained cell lines expressing endogenous SUMOylation deficient mutant KIF4A. To the best of our knowledge this is the first time this technique was employed to study a SUMO target protein at the endogenous level, which avoids the risks of incorrect and heterogeneous expression levels of exogenous constructs. Moreover, it overcomes the challenge of missing out on potential phenotypes due to partial knockdown. Clearly, CRISPR-Cas9 genome editing should gain momentum to reveal the functional relevance of specific post-translational modification events in the SUMO field and beyond.

By mutating a single lysine in KIF4A, we were able to reveal a specific function of SUMO-modified KIF4A in abscission. Previous research using silencing techniques claimed a role of the multifunctional KIF4A protein earlier in mitosis. In this case, the function of KIF4A in abscission was missed out because this stage of mitosis is not properly reached in the absence of KIF4A. Our study indicates that additional functions might be uncovered for other proteins by focusing on the modification level rather than the total protein level. Investigating proteins regulated by post-translational modification at this level is challenging. Interestingly,

our results show that SUMO is able to regulate key cellular functions by the modification of single target proteins in addition to its role in protein group modification (Psakhye and Jentsch, 2012). As a result of co-regulation of functional groups by SUMOylation, phenotypes of single target proteins deficient for SUMOylation are generally modest and quite often, no phenotypes can be found at all.

SUMOylation levels of KIF4A appeared to be rather stable during cell cycle progression, indicating that KIF4A is continuously modified and demodified at constant rates throughout the cell cycle. This is a fairly puzzling finding, but also intriguing and novel, showing that a stable modification has a function at a specific phase of mitosis, i.e. abscission. This could be due to limited opportunities for the enzymatic machinery to carry out the modification during cytokinesis. One thought here is that the SUMO conjugating machinery is equipped with DNA binding domains, limiting SUMO conjugation primarily to the presence of substrates at chromatin. Therefore, the modification has to happen prior to cytokinesis, despite its function in abscission.

We have uncovered a novel role for SUMOylated KIF4A in cytokinesis, playing a role in abscission. The process of cytokinesis is tightly regulated to ensure daughter cells are not separated until sister chromatid segregation is completed. We now place SUMO modification of KIF4A and the resulting association with STMN1 in a dynamic model that is critical in the last phase of mitosis, as shown in Fig. 7. How dynamic modification by SUMO of KIF4A is controlled during mitosis is unclear. But a complex SUMO-controlled event determines the last step in mitosis.

Materials and methods

CRISPR-Cas9-directed genome editing

To obtain cell lines in which the triplet encoding lysine 460 in the endogenous KIF4A was replaced by a triplet encoding arginine, CRISPR-Cas9-directed genome editing was used in combination with a repair template enabling targeted mutagenesis. The pSpCas9(BB)-2A-GFP plasmid (Ran et al., 2013) was digested with BbsI (New England Biolabs) and purified from a 1% TAE agarose gel using the Wizard® SV Gel and PCR Clean-up System (Promega). Two guide RNA primers were designed containing BbsI overhangs and the target sequence upstream of the selected Protospacer adjacent motif (PAM) region close to the sequence encoding lysine 460 (forward (FW): 5' CACCGAGTGGAGACTTTGGAAGACC 3' and reverse (RV): 5' AAACGGTCTTCCAAAGTCTCCACTC 3'). These primers were annealed and phosphorylated by T4 polynucleotide kinase (New England Biolabs), before ligation into the BbsI digested plasmid by T4 ligase (New England Biolabs). A repair template was designed to contain the desired lysine to arginine mutation and several silent mutations to prevent recognition of the repaired gene by the guide RNA and to introduce a recognition site for the restriction enzyme TaqαI (5' GTCATATGAATAACCCTTGGGTTCTTTTTGTTTGAATTTTCAGCTGCAAACTGGATCTTC AAAAGCTTGTCGAGACATTGGAGGATCAGGAATTGAGAGAAAATGTAGAGATAATTTGT AACCTGCAGCAATTGATTACCCAGTTATCGGTAAGCCAAGTAGGGGCAGTGTAAAT 3'), and obtained as 4 nmole ultramer (Integrated DNA Technologies). Two million U2OS cells were transfected with 3 µg of Cas9/GFP/guideRNA encoding plasmid and 6 µl of 10 µM repair template using 14.4 µl Lipofectamine 2000 (Invitrogen) in Optimem (Life Technologies). Three days after transfection, cells were sorted by flow cytometry and GFP positive cells were plated at 5000 cells per 15 cm dish. Colonies were picked and maintained in 24 well plates. DNA was purified from each clone and part of the KIF4A gene was amplified by PCR using GoTaq polymerase (Promega) and the following primers: FW 5' ACCGCCACTGATGATCTCCTG 3' and RV 5' ATCAAATGATCCACGACCTCTGTCC 3'. The PCR product was digested by TaqαI

(New England Biolabs) to determine which cells had used the designed template to repair the break caused by Cas9. Candidate clones and several control clones were sequenced to confirm their identity. This procedure was repeated until three correctly mutated clones were identified. Each mutant clone was matched to a clone that had undergone exactly the same procedure but was identified with a sequence encoding wildtype (WT) KIF4A, resulting in three individual sets of a WT and a K460R clone.

Cell culture and cell lines

Unless otherwise stated, human embryonic kidney 293 (HEK293T) cells (DuBridge et al., 1987) and human bone osteosarcoma epithelial (U2OS) cells (ATCC) were cultured at 37°C and 5% CO_2 in Dulbecco's modified eagle's medium (DMEM, Thermo Fisher Scientific) supplemented with 10% fetal bovine serum (FBS, Thermo Fisher Scientific), 100 U/ml penicillin and 100 µg/ml streptomycin (P/S, Thermo Fisher Scientific). Cells were authenticated and regularly tested for mycoplasma infection and found to be negative. The U2OS cell line stably expressing low levels of His_{10}-tagged SUMO2 was obtained by infection with a lentivirus encoding a His_{10}-SUMO2 IRES GFP construct and subsequent selection by low GFP expression as described before (Hendriks et al., 2014). The mature protein that is referred to as SUMO2 has the following amino acid sequence:MSEEKPKEGVKTENDHINLKVAGQDGSVVQFKIKRHTPLSKLMKAYCERQGLSM RQIRFRFDGQPINETDTPAQLEMEDEDTIDVFQQQTGG.

To enable enrichment of SUMOylated endogenous proteins from the three sets of KIF4A WT and K460R clones, the cell lines were infected with lentivirus encoding His_{10}-SUMO2 and puromycin resistance (Hendriks and Vertegaal, 2016b) at an MOI of 3 using 8 µg/ml polybrene. Stable His_{10}-SUMO2 expressing cell lines were created by selection with 2.5 µM puromycin (Calbiochem). To enable visualization of microtubules by live cell imaging, the three sets of KIF4A WT and K460R clones were transfected with the pEGFP containing α-tubulin plasmid (Clontech). After selection by Geneticin (G418, Life Technologies), cells were

seeded at 5000 cells per 15 cm dish. GFP-positive colonies were picked based on equal expression levels and additionally sorted by flow cytometry.

Site-directed mutagenesis

Mutations were introduced in the WT KIF4A construct encoding the canonical KIF4A protein (Uniprot identifier: O95239-1) using QuickChange site-directed mutagenesis (Stratagene). The forward and reverse primers used were: K460R FW 5' GACCAGGAATTGAGAGAAAATGTAGAG 3', K460R RV 5' CTCTACATTTTCTCTCAATTCCTGGTC 3', E458A FW 5' GTGGAGACTTTGGAAGACCAGGCGTTGAAAGAAAATGTAGAG 3', E458A RV 5' CTCTACATTTTCTTTCAACGCCTGGTCTTCCAAAGTCTCCAC 3', E461A FW 5' GGAAGACCAGGAATTGAAAGCGAATGTAGAGATAATTTG 3', E461A RV 5' CAAATTATCTCTACATTCGCTTTCAATTCCTGGTCTTCC 3', E458/461A FW 5' CTTTGGAAGACCAGGCGTTGAAAGCGAATGTAGAG 3', E458/461A RV 5' CTCTACATTCGCTTTCAACGCCTGGTCTTCCAAAG 3', ΔSIM FW 5' CTGAAAGTGTCTTACTTAGAGATTTACAATGAAGAAGCTGCGGATGCTGCATGCCCATC TCGTGAGAAAGC 3' and ΔSIM RV 5' GCTTTCTCACGAGATGGGCATGCAGCATCCGCAGCTTCTTCATTGTAAATCTCTAAGTA AGACACTTTCAG 3'.

Transfection and lentivirus production

Cells were plated in FBS containing DMEM without P/S. To obtain overexpression of the indicated protein, U2OS cells were transfected with 24 µg plasmid DNA and 60 µg polyethylaneimine (PEI) at 60% confluency in a 15 cm dish. Medium was replaced for DMEM containing FBS and P/S after 24 hours and cells were washed with PBS and lysed three days after transfection to obtain total lysate samples (input) and samples for protein purification (His_{10}-pulldown or HA-immunoprecipitation) unless otherwise stated. To produce lentivirus,

HEK293T cells were transfected with 7.5 µg pCMV-VSVG, 11.4 µg pMDLg-RRE, 5.4 µg pRSV-REV and 13.7 µg of a plasmid encoding SUMO2 as well as puromycin resistance. The medium was collected 48 and 72 hours after transfection and filtered using a 0.45 µm syringe filter (Pall Life Science). The virus titer was determined using p24 elisa and the sample was stored at -20°C until use.

His_{10}-pulldown

Enrichment of SUMOylated proteins was performed by His_{10}-pulldown as described before (Hendriks et al., 2014). In short, cells were resuspended in lysis buffer, sonicated and equalized using BCA Protein Assay Reagent (Thermo Fisher Scientific). Lysates were incubated with Ni-NTA beads (Qiagen) overnight at 4°C, washed and eluted for 30 minutes at room temperature (RT).

HA-immunoprecipitation

To detect modification of exogenous HA-tagged KIF4A to endogenous SUMO2/3, an HA-immunoprecipitation (IP) was performed to preserve SUMOylation on target proteins according to the following protocol. Cells were lysed in buffer 1, containing 1% SDS, 0.5% NP-40, 50 mM NaF, 1 mM $NaVO_3$, 5 mM β-glycerol phosphate, 5 mM NaPy, 0.5 mM EGTA, 5 mM PNT, protease inhibitors with EDTA, 70 mM chloroacetamide (CAA) and 1x PBS. Samples were equalized using BCA Protein Assay Reagent and diluted with an equal volume of buffer 2 (2% Triton-X100, 0.5% sodium deocxycholate, 1% BSA, 5 mM NaF, 1 mM $NaVO_3$, 5 mM β-glycerol phosphate, 5 mM NaPy, 0.5 mM EGTA, 5 mM PNT, protease inhibitors with EDTA, 70 mM CAA and 1x PBS). Upon centrifugation at 4°C and 13200 rpm for 45 minutes, the supernatant was collected and incubated with Ezview Red Anti-HA Affinity Gel (Sigma) for 90 minutes at 4°C while moving. Samples were washed four times with buffer 3, containing 50 mM Tris (pH 7.5), 150 mM NaCl, 0.5% NP-40, 5 mM NaF, 1 mM $NaVO_3$, 5 mM β-glycerol phosphate, 5 mM NaPy, 0.5 mM EGTA, 5 mM PNT, protease inhibitors with EDTA and 70 mM CAA. Next, samples were washed twice with buffer 4, containing 50 mM Tris (pH 7.5), 150

mM NaCl and 0.5% NP-40. Finally, samples were eluted for 30 minutes at RT and 1200 rpm in buffer 4 supplemented with 100 µg/ml HA-peptide (Sigma).

To purify HA-tagged KIF4A for *in vitro* SUMOylation reactions, an HA-IP was performed in a non-denaturing manner according to the following protocol. Cells were lysed in buffer 5, containing 30 mM HEPES (pH 7.6), 130 mM NaCl, 1 mM $MgCl_2$, 0.5% Triton-X100, protease inhibitors with EDTA and 70 mM CAA. Samples were incubated on ice for 10 minutes, before centrifugation at 4°C and 15000 rcf for 10 minutes. The supernatant was collected and equalized using BCA Protein Assay Reagent. After incubation with Ezview Red Anti-HA Affinity Gel for 90 minutes at 4°C while rotating, samples were washed six times in buffer 5. Finally, samples were eluted in buffer 5 supplemented with 100 µg/ml HA-peptide at RT and 1200 rpm for 30 minutes.

SUMOylation of eluted HA-KIF4A

HA-KIF4A enriched from four million U2OS cells by HA-IP as described above was *in vitro* SUMOylated. Unless otherwise stated, samples were incubated in a total volume of 20 µl for 3 hours at 4°C with SUMOylation mix, containing 50 mM Tris (pH 7.5), 5 mM $MgCl_2$, 3.5 U/ml creatine kinase, 10 mM creatine phosphate, 1.1 U/ml inorganic pyrophosphatase, 2 mM ATP, 600 ng SUMO E1, 2 µg SUMO E2 and 4.4 µg SUMO2 Kzero (K0). SUMO2 K0 refers to a mutant SUMO2 in which all lysines are mutated into arginines to prevent SUMO chain formation.

Electrophoresis, immunoblotting and antibodies

For each experiment the collected cells were divided in at least two aliquots, including one for total lysate samples (input) and one for protein purification (His_{10}-pulldown or HA-IP). Inputs were lysed in input buffer (1% SDS, 1% NP-40, 50 mM Tris (pH 7.5) and 150 mM NaCl), incubated at 99°C for 10 minutes at 1200 rpm and equalized using BCA Protein Assay Reagent, followed by immunoblot analysis. Purification samples were prepared according to the His_{10}-pulldown or HA-IP protocol. For immunoblot analysis, dithiothreitol (DTT, Sigma) and

NuPAGE LDS Sample Buffer (LDS, Life Technologies) were added and each sample was incubated at 70°C for 10 minutes. Proteins were separated by gel electrophoresis on home-made 8% or 15% gels in Tris-glycine buffer for 75 minutes at 150 Volt. Proteins were transferred to Hybond nitrocellulose membranes (GE Healthcare) in cold transfer buffer at 25V for 3 hours. Subsequently, proteins were stained with Ponceau S (Sigma) to confirm equal loading and membranes were blocked in PBS with 0.05% Tween-20 (Merck) and 8% milk powder (blocking solution) for one hour at RT. Membranes were incubated overnight at 4°C with primary antibodies diluted in blocking solution, including rabbit polyclonal anti-KIF4A (Bethyl, A301-074A, 1:2000), mouse monoclonal anti-SUMO2/3 (Abcam, 8A2, 1:2000), mouse monoclonal anti-HA.11 (Sanbio, MMS-101R, 1:1000), mouse monoclonal anti-α-tubulin (Sigma, T6199, 1:1000), rabbit polyclonal anti-GFP (Novus Biologicals, NB600-308, 1:1000) and rabbit monoclonal anti-STMN1 (Cell Signaling Technology, D1Y5A, 1:1000). Membranes were washed three times for 10 minutes at RT in PBS containing 0.05% Tween-20 (PBS/T), before incubation with HRP-coupled secondary antibodies donkey anti-rabbit or goat anti-mouse (Pierce) diluted in blocking solution for one hour at 4°C. Upon washing in PBS/T three times for 10 minutes at 4°C, Pierce ECL 2 immunoblotting substrate (Life Technologies) was used to visualize the signal on RX Medical films (Fuji).

Cell synchronization and fluorescence-activated cell sorting analysis

Two blocking agents were used to synchronize cells into specific cell cycle stages. Thymidine (Sigma) was added at a concentration of 4 mM to block cells at the border of G1 to S phase. After 16 hours, cells were lysed immediately (G1 phase) or washed twice with PBS to release them from their cell cycle arrest. These cells were either released into DMEM with FBS and P/S for 5 hours (early S phase) or 8 hours (late S phase) or into DMEM with FBS, P/S and 0.1 µg/ml nocodazole (Sigma) to block cells in prometaphase. After 20 hours these arrested cells were lysed immediately (early M phase) or released into DMEM with FBS and P/S for 30 minutes (mid M phase), 2 hours (late M phase), 4 hours (G1 phase) or 8 hours (G1/S phase). Cells were collected using trypsin treatment and washed with PBS. Finally, each sample was

divided into three aliquots, which were fixed for fluorescence-activated cell sorting (FACS) analysis, lysed to perform a His_{10}-pulldown or lysed to obtain input samples.

The samples harvested for FACS analysis were fixed in 70% ice-cold ethanol and incubated at 4°C for at least 16 hours. Samples were prepared on the day of measurement by flow cytometry, starting with centrifugation at 1200 rpm for 2 minutes and washing in PBS with 2% FBS. Upon a second centrifugation step, cells were resuspended in PBS containing 2% FBS, 25 µg/ml propidium iodide (Sigma) and 100 µg/ml RNAse A (Sigma). Samples were stained for 30 minutes at 37°C, followed by measuring the cellular DNA content by flow cytometry with the BD LSRII system and BD FACS DIVA software (BD Bioscience Clontech).

ATPase activity assay

Recombinant GST-KIF4A wildtype (WT) or SUMO deficient mutants (K460R and E458/461E) were *in vitro* SUMOylated by incubation at 4°C for 3 hours. The complete SUMOylation mix used for one ATPase activity reaction contained 2.5 µg GST-KIF4A, 750 ng SUMO E1, 2.5 µg SUMO E2 and 5.5 µg SUMO2 K0 in 50 mM Tris (pH 7.5), 5 mM $MgCl_2$ and 2 mM ATP (dissolved in PIPES). As a non-SUMOylated control, the same reaction was taken along, omitting SUMO2 K0. Aliquots of all SUMOylation reactions were saved for immunoblot analysis. To measure ATPase activity the Kinesin ATPase end-point assay (Cytoskeleton) was used according to manufacturer's instructions, except for the use of 300 µl wells and therefore doubling all reaction volumes. As an additional control, all experimental conditions were also incubated in the absence of microtubules (MTs) to determine background activity. Absorbance was measured at 650 nm with a Synergy HT spectrophotometer (BioTek). Three independent experiments were performed and average relative absorbance with standard deviations were calculated. The two-sided Student T-test was used to determine p values.

Immunofluorescence

All three sets of WT and K460R KIF4A clones were plated on glass slides in 24 well plates. After two days, cells were fixed for 15 minutes at RT in 4% PFA and washed four times in

PBS. Cells were permeabilized by 1% Triton-X100 in PBS for 15 minutes at RT, followed by washing twice with PBS and once with PBS/T. Samples were blocked for 10 minutes in TNB, containing 100 mM Tris (pH 7.5), 150 mM NaCl and 0.5% blocking reagent (Roche). After incubation for one hour at RT with primary antibodies against KIF4A and tubulin diluted in TNB, coverslips were washed five times with PBS/T. Then, cells were incubated for one hour at RT with secondary antibodies (Alexa-488 goat anti-mouse and Alexa-594 goat anti-rabbit) diluted in TNB and washed five time with PBS/T. Coverslips were dehydrated by incubating for one minute each with 70%, 90% and 100% ethanol. Finally, coverslips were mounted onto a microscopy slide using ProLong Gold (Life Technologies) containing 5 µg/ml Hoechst 33258 (Life Technologies).

For high resolution pictures, mitotic cells were visualized using a Leica TCS SP8 confocal microscope with a 63x objective. Z-stacks were made of cells from top to bottom with 0.4 µm steps at a 1024x1024 format with a speed of 100 Hz. Finally, maximum projections were made and shown in the figures. To determine the percentage of mitotic cells, random images were taken on a Leica DM6B fluorescence microscope. The numbers of total cells and of mitotic cells were analysed per image for at least 400 cells per clone per experiment. The percentage of cells in mitosis and in each subphase was calculated for six independent experiments and averaged for each clone. The means with standard deviations are shown in the supplementary figures. The results for the three WT and three K460R cell lines were averaged, for which the data with standard deviations are shown in the main figures. The two-sided Student T-test was used to calculate p values.

Live cell imaging

Cells were grown on glass bottomed imaging chambers CG (Zell-Kontakt) in DMEM supplemented with FBS and P/S at 37°C in a humidified atmosphere containing 5% CO_2. Before imaging, the medium was changed to phenol red free CO_2-independent Leibovitz's L-15 medium (Thermo Fisher Scientific) supplemented with FBS and the lid was exchanged for a DIC lid (Zell-Kontakt). Movies were acquired using the Eclipse Ti wide-field microscope

(Nikon) with a Plan Apo λ 60x NA 1.4 objective at 37°C in an environment chamber. Five optical sections were collected every 1.5 µm using the ORCA-Flash 4.0 CMOS camera C11440-22CU (Hamamatsu). 2x2 binning was applied for increased signal intensity.

To determine timing from anaphase onset to abscission, mitotic progression of 66 cells per WT clone and of 51 cells per K460R clone was analyzed using Image J software version 1.50e. Anaphase onset was determined as the first frame in which the start of chromosome segregation was visible by DIC. These cells were followed while continuing mitosis until the intercellular microtubule bridge was disconnected at the end of cytokinesis and this frame was marked as the moment of abscission. The timing from anaphase onset to abscission for each individual cell is represented by a colored triangle, while the medians with interquartile ranges are shown in black. The results for the individual clones are shown in the supplementary figure, while the main figure shows all 198 WT and 153 K460R cells analysed from the individual clones pooled together. The Mann Whitney test was used to calculate p values.

Identification of GST-KIF4A binders by mass spectrometry and data analysis

An *in vitro* SUMOylation reaction was performed for 3 hours at 4°C with 10 µg recombinant WT or K460R GST-KIF4A in buffer containing 50 mM Tris (pH 7.5), 5 mM $MgCl_2$, 2 mM ATP, 3 µg SUMO E1, 10 µg SUMO E2 and 20 µg SUMO K0. The same buffer conditions, except for the absence of SUMO K0, were used as an additional negative control. Samples were incubated with Glutathione Sepharose 4 Fast Flow beads (GE Healthcare) for one hour at 4°C, followed by washing twice with buffer 6 (50 mM Tris (pH 7.5) and 150 mM NaCl). Subsequently, samples were incubated for two hours at 4°C with U2OS cell lysate. Lysates were prepared in buffer containing 50 mM Tris (pH 7.5), 150 mM NaCl, 0.5% Triton-X100, 10 mM N-Ethylmaleimide (NEM, Sigma) and protease inhibitors with EDTA. After washing three times with buffer 6, samples were washed three times with 50 mM ammonium bicarbonate (ABC, Sigma) and eluted for 30 minutes at RT and 1200 rpm in ABC complemented with 20 mM glutathione (Sigma).

Samples were passed through pre-washed 0.45 µm filter columns to remove the beads and digested by incubation with 2 µg trypsin (Promega) overnight at 37°C and 500 rpm. To acidify the samples, trifluoroacetic acid (TFA, Sigma) was added to a final concentration of 2%. Stage tips containing C18 (Sigma) were activated by passing HPLC-grade methanol (Sigma), washed with 80% acetonitrile (ACN, Sigma) in 0.1% formic acid (FA, Sigma) and equilibrated with 0.1% FA. Samples were loaded on these stage tips, washed twice with 0.1% FA and eluted twice with 80% ACN. Finally, samples were vacuum dried using a SpeedVac RC10.10 (Jouan), redissolved in 0.1% FA and transferred to autoloader vials before measurement by mass spectrometry. Four independent experiments were performed and all samples were measured by nanoflow liquid chromatography-tandem mass spectrometry (nanoLC-MS/MS) on an EASY-nLC 1000 system (Proxeon) connected to an Orbitrap Q-Exactive (Thermo Fisher Scientific) through a nano-electrospray ion source. Raw data analysis was performed using Max Quant Software version 1.5.3.30 with its integrated search engine Andromeda. The search was performed against the *in silico* digested proteome containing 92180 entries of *Homo sapiens* from UniProt (24th March 2016). Label-free quantification was performed using LFQ settings with fast LFQ disabled to quantify all identified peptides (Supplementary information, Tables S1 and S2). Proteins identified by the same set of peptides were combined to a single protein group by Max Quant (Supplementary information, Tables S1 and S3). These protein groups were further analysed using Perseus Software version 1.5.2.4. Proteins identified in the categories 'potential contaminant', 'reverse' or 'only identified by site' were removed. The LFQ intensities were log2 transformed and the experimental replicates for each condition were assigned together in an experimental group. Subsequently, all proteins that were not identified in each experimental replicate of at least one experimental group were removed. Missing values were imputed based on the total matrix, using normally distributed values with a randomized 0.3 width (log2) and a 1.8 down shift (log2). Two-sided Student T-tests were performed between the indicated samples to obtain p values and differences for each protein. These values were visualized in a volcano plot, showing p values (as -Log10(p)) on the y-axis and differences (as Log2FC (fold change))

on the x-axis. All proteins with a p value below 0.05 were considered to bind significantly different between the two indicated experimental groups (Supplementary information, Tables S1 and S4).

GST-STMN1 binding to HA-KIF4A

Three days after transfection of U2OS cells with control or HA-KIF4A WT plasmid, cells were lysed in buffer 7 (50 mM Tris (pH 7.5), 5 mM $MgCl_2$, 150 mM NaCl and 0.5% Triton-X100). Samples were sonicated and centrifuged at 15000 rcf for 30 minutes at 4°C. Upon collection of the supernatant, BCA Protein Assay Reagent was used to equalize the samples. Then, samples were incubated with Ezview Red Anti-HA Affinity Gel for 90 minutes at 4°C and washed twice in buffer 7. Upon washing twice in buffer 8 (50 mM Tris (pH 7.5) and 5 mM $MgCl_2$), an *in vitro* SUMOylation reaction was performed on the beads containing HA-KIF4A enriched from one million U2OS cells for 3 hours at 4°C while moving in a total reaction volume of 50 µl containing 50 mM Tris (pH 7.5), 5 mM $MgCl_2$, 4 mM ATP, 1.5 µg SUMO E1, 5 µg SUMO E2 and 10 µg SUMO K0. Samples were washed for three times with buffer 6, followed by incubation with 1 µg recombinant GST-STMN1 WT for 2 hours at 4°C while moving. Finally, samples were washed in buffer 7 and eluted in buffer 7 supplemented with 100 µg/ml HA-peptide at RT and 1200 rpm for 30 minutes. After performing electrophoresis and immunoblotting as described above, the obtained signal was quantified using Fiji version 2.0.0. Three independent experiments were performed and average relative binding with standard deviations were calculated. The two-sided Student T-test was used to determine p values.

Acknowledgements

We thank Dr. K. Eifler and Dr. J. Schimmel for advice as well as Dr. I. Hendriks and Dr. R. González-Prieto for help with mass spectrometry. We thank Dr. J.J.C. Neefjes for excellent comments on the manuscript. This work was supported by the European Research Council (ERC, grant number 310913), the Netherlands Organization for Scientific Research (NWO), the Dutch Cancer Society (grant number 10835) (A.C.O.V.), the Wellcome Trust, of which W.C.E. is a Principal Research Fellow (grant number 107022) and the Marie Curie Action PloidyNet (J.G.R.), funded by the European Union FP7/2007-2013 under grant agreement number 607722.

Competing interests

No competing interests declared.

Data availability

The mass spectrometry proteomics data have been deposited to the ProteomeXchange Consortium via the PRIDE (Vizcaino et al., 2016) partner repository with the dataset identifier PXD007055.

References

Barr, F. A., Sillje, H. H. and Nigg, E. A. (2004). Polo-like kinases and the orchestration of cell division. *Nat. Rev. Mol. Cell Biol.* 5, 429-440.

Bernier-Villamor, V., Sampson, D. A., Matunis, M. J. and Lima, C. D. (2002). Structural basis for E2-mediated SUMO conjugation revealed by a complex between ubiquitin-conjugating enzyme Ubc9 and RanGAP1. *Cell* 108, 345-356.

Connell, J. W., Lindon, C., Luzio, J. P. and Reid, E. (2009). Spastin couples microtubule severing to membrane traffic in completion of cytokinesis and secretion. *Traffic.* 10, 42-56.

Cubenas-Potts, C., Srikumar, T., Lee, C., Osula, O., Subramonian, D., Zhang, X. D., Cotter, R. J., Raught, B. and Matunis, M. J. (2015). Identification of SUMO-2/3-modified proteins associated with mitotic chromosomes. *Proteomics.* 15, 763-772.

Dasso, M. (2008). Emerging roles of the SUMO pathway in mitosis. *Cell Div.* 3, 5.

DuBridge, R. B., Tang, P., Hsia, H. C., Leong, P. M., Miller, J. H. and Calos, M. P. (1987). Analysis of mutation in human cells by using an Epstein–Barr virus shuttle system. *Mol. Cell Biol.* 7, 379–387.

Deribe, Y. L., Pawson, T. and Dikic, I. (2010). Post-translational modifications in signal integration. *Nat. Struct. Mol. Biol.* 17, 666-672.

Eifler, K. and Vertegaal, A. C. (2015). SUMOylation-Mediated Regulation of Cell Cycle Progression and Cancer. *Trends Biochem. Sci.* 40, 779-793.

Field, C. M. and Alberts, B. M. (1995). Anillin, a contractile ring protein that cycles from the nucleus to the cell cortex. *J. Cell Biol.* 131, 165-178.

Flotho, A. and Melchior, F. (2013). Sumoylation: a regulatory protein modification in health and disease. *Annu. Rev. Biochem.* 82, 357-385.

Fu, C., Ahmed, K., Ding, H., Ding, X., Lan, J., Yang, Z., Miao, Y., Zhu, Y., Shi, Y., Zhu, J. et al. (2005). Stabilization of PML nuclear localization by conjugation and oligomerization of SUMO-3. *Oncogene* 24, 5401-5413.

Gareau, J. R. and Lima, C. D. (2010). The SUMO pathway: emerging mechanisms that shape specificity, conjugation and recognition. *Nat. Rev. Mol. Cell Biol.* 11, 861-871.

Glotzer, M., Murray, A. W. and Kirschner, M. W. (1991). Cyclin is degraded by the ubiquitin pathway. *Nature* 349, 132-138.

Guizetti, J., Schermelleh, L., Mantler, J., Maar, S., Poser, I., Leonhardt, H., Muller-Reichert, T. and Gerlich, D. W. (2011). Cortical constriction during abscission involves helices of ESCRT-III-dependent filaments. *Science* 331, 1616-1620.

Gurley, L. R., Walters, R. A. and Tobey, R. A. (1973). Histone phosphorylation in late interphase and mitosis. *Biochem. Biophys. Res. Commun.* 50, 744-750.

Guttinger, S., Laurell, E. and Kutay, U. (2009). Orchestrating nuclear envelope disassembly and reassembly during mitosis. *Nat. Rev. Mol. Cell Biol.* 10, 178-191.

Hayashi, T., Seki, M., Maeda, D., Wang, W., Kawabe, Y., Seki, T., Saitoh, H., Fukagawa, T., Yagi, H. and Enomoto, T. (2002) Ubc9 is essential for viability of higher eukaryotic cells. *Exp Cell Res*. 280, 212-221.

He, X., Riceberg, J., Pulukuri, S. M., Grossman, S., Shinde, V., Shah, P., Brownell, J. E., Dick, L., Newcomb, J. and Bence, N. (2015). Characterization of the loss of SUMO pathway function on cancer cells and tumor proliferation. *PLoS One* 10, e0123882.

Hendriks, I. A., D'Souza, R. C., Yang, B., Verlaan-de Vries, M., Mann, M. and Vertegaal, A. C. (2014). Uncovering global SUMOylation signaling networks in a site-specific manner. *Nat. Struct. Mol. Biol.* 21, 927-936.

Hendriks, I. A. and Vertegaal, A. C. (2016a). A comprehensive compilation of SUMO proteomics. *Nat. Rev. Mol. Cell Biol.* 17, 581-595.

Hendriks, I. A. and Vertegaal, A. C. (2016b). A high-yield double-purification proteomics strategy for the identification of SUMO sites. *Nat. Protoc.* 11, 1630-1649.

Hu, C., Coughlin, M., Field, C.M., Mitchison, T.J. (2011) KIF4 regulates midzone length during cytokinesis. *Curr. Biol.* 21, 815-824.

Joo, E., Surka, M. C. and Trimble, W. S. (2007). Mammalian SEPT2 is required for scaffolding nonmuscle myosin II and its kinases. *Dev. Cell* 13, 677-690.

King, R. W., Deshaies, R. J., Peters, J. M. and Kirschner, M. W. (1996). How proteolysis drives the cell cycle. *Science* 274, 1652-1659.

King, R. W., Jackson, P. K. and Kirschner, M. W. (1994). Mitosis in transition. *Cell* 79, 563-571.

Kurasawa, Y., Earnshaw, W. C., Mochizuki, Y., Dohmae, N. and Todokoro, K. (2004). Essential roles of KIF4 and its binding partner PRC1 in organized central spindle midzone formation. *EMBO J.* 23, 3237-3248.

Larsson, N., Marklund, U., Gradin, H. M., Brattsand, G. and Gullberg, M. (1997). Control of microtubule dynamics by oncoprotein 18: dissection of the regulatory role of multisite phosphorylation during mitosis. *Mol. Cell Biol.* 17, 5530-5539.

Lee, Y. M. and Kim, W. (2004). Kinesin superfamily protein member 4 (KIF4) is localized to midzone and midbody in dividing cells. *Exp. Mol. Med.* 36, 93-97.

Lewellyn, L., Carvalho, A., Desai, A., Maddox, A. S. and Oegema, K. (2011). The chromosomal passenger complex and centralspindlin independently contribute to contractile ring assembly. *J. Cell Biol.* 193, 155-169.

Li, S. J. and Hochstrasser, M. (1999). A new protease required for cell-cycle progression in yeast. *Nature* 398, 246-251.

Mabuchi, I. (1994). Cleavage furrow: timing of emergence of contractile ring actin filaments and establishment of the contractile ring by filament bundling in sea urchin eggs. *J. Cell Sci.* 107 (Pt 7), 1853-1862.

Matic, I., Schimmel, J., Hendriks, I. A., van Santen, M. A., van de Rijke, F., van Dam, H., Gnad, F., Mann, M. and Vertegaal, A. C. (2010). Site-specific identification of SUMO-2 targets in cells reveals an inverted SUMOylation motif and a hydrophobic cluster SUMOylation motif. *Mol. Cell* 39, 641-652.

Mavrakis, M., Azou-Gros, Y., Tsai, F. C., Alvarado, J., Bertin, A., Iv, F., Kress, A., Brasselet, S., Koenderink, G. H. and Lecuit, T. (2014). Septins promote F-actin ring formation by crosslinking actin filaments into curved bundles. *Nat. Cell Biol.* 16, 322-334.

Mierzwa, B. and Gerlich, D. W. (2014). Cytokinetic abscission: molecular mechanisms and temporal control. *Dev. Cell* 31, 525-538.

Mullins, J. M. and Biesele, J. J. (1977). Terminal phase of cytokinesis in D-98s cells. *J. Cell Biol.* 73, 672-684.

Nacerddine, K., Lehembre, F., Bhaumik, M., Artus, J., Cohen-Tannoudji, M., Babinet, C., Pandolfi, P. P. and Dejean, A. (2005). The SUMO pathway is essential for nuclear integrity and chromosome segregation in mice. *Dev. Cell* 9, 769-779.

Nie, M. and Boddy, M. N. (2016). Cooperativity of the SUMO and Ubiquitin Pathways in Genome Stability. *Biomolecules.* 6.

Nouar, R., Breuzard, D., Bastonero, S., Gorokhova, S., Barbier, P., Devred, F., Kovacic, H. and Peyrot, V. (2016) Direct evidence for the interaction of Stathmin anlong the length and the plus end of microtubules in cells. *FASEB J.* 30, 3202-3215.

Nunnally, M. H., D'Angelo, J. M. and Craig, S. W. (1980). Filamin concentration in cleavage furrow and midbody region: frequency of occurrence compared with that of alpha-actinin and myosin. *J. Cell Biol.* 87, 219-226.

Pelisch, F., Tammsalu, T., Wang, B., Jaffray, E. G., Gartner, A. and Hay, R. T. (2017). A SUMO-Dependent Protein Network Regulates Chromosome Congression during Oocyte Meiosis. *Mol. Cell* 65, 66-77.

Peters, J. M. (2002). The anaphase-promoting complex: proteolysis in mitosis and beyond. *Mol. Cell* 9, 931-943.

Pichler, A., Fatouros, C., Lee, H. and Eisenhardt, N. (2017). SUMO conjugation - a mechanistic view. *Biomol. Concepts* 8, 13-36.

Pichler, A., Knipscheer, P., Oberhofer, E., van Dijk, W. J., Korner, R., Olsen, J. V., Jentsch, S., Melchior, F. and Sixma, T. K. (2005). SUMO modification of the ubiquitin-conjugating enzyme E2-25K. *Nat. Struct. Mol. Biol.* 12, 264-269.

Pohl, C. and Jentsch, S. (2008). Final stages of cytokinesis and midbody ring formation are controlled by BRUCE. *Cell* 132, 832-845.

Psakhye, I. and Jentsch, S. (2012). Protein group modification and synergy in the SUMO pathway as exemplified in DNA repair. *Cell* 151, 807-820.

Ran, F. A., Hsu, P. D., Wright, J., Agarwala, V., Scott, D. A. and Zhang, F. (2013). Genome engineering using the CRISPR-Cas9 system. *Nat. Protoc.* 8, 2281-2308.

Reichl, E. M., Ren, Y., Morphew, M. K., Delannoy, M., Effler, J. C., Girard, K. D., Divi, S., Iglesias, P. A., Kuo, S. C. and Robinson, D. N. (2008). Interactions between myosin and actin crosslinkers control cytokinesis contractility dynamics and mechanics. *Curr. Biol.* 18, 471-480.

Ribet, D., Boscaini, S., Cauvin, C., Siguier, M., Mostowy, S., Echard, A. and Cossart, P. (2017) SUMOylation of human septins is critical for septin filament bundling and cytokinesis. *J Cell Biol.* 216, 4041-4052.

Sanger, J. M., Dome, J. S., Hock, R. S., Mittal, B. and Sanger, J. W. (1994). Occurrence of fibers and their association with talin in the cleavage furrows of PtK2 cells. *Cell Motil. Cytoskeleton* 27, 26-40.

Schimmel, J., Eifler, K., Sigurðsson, J. O., Cuijpers, S. A., Hendriks, I. A., Verlaan-de Vries, M., Kelstrup, C. D., Francavilla, C., Medema, R. H., Olsen, J. V. et al. (2014). Uncovering SUMOylation Dynamics during Cell-Cycle Progression Reveals FoxM1 as a Key Mitotic SUMO Target Protein. *Mol. Cell* 53, 1053-1066.

Schroeder, T. E. (1968). Cytokinesis: filaments in the cleavage furrow. *Exp. Cell Res.* 53, 272-276.

Seeler, J. S. and Dejean, A. (2017). SUMO and the robustness of cancer. *Nat. Rev. Cancer* 17, 184-197.

Seufert, W., Futcher, B. and Jentsch, S. (1995). Role of a ubiquitin-conjugating enzyme in degradation of S- and M-phase cyclins. *Nature* 373, 78-81.

Teixeira, L. K. and Reed, S. I. (2013). Ubiquitin ligases and cell cycle control. *Annu. Rev. Biochem.* 82, 387-414.

Uehara, R., Goshima, G., Mabuchi, I., Vale, R. D., Spudich, J. A. and Griffis, E. R. (2010). Determinants of myosin II cortical localization during cytokinesis. *Curr. Biol.* 20, 1080-1085.

Vizcaino, J. A., Csordas, A., del-Toro, N., Dianes, J. A., Griss, J., Lavidas, I., Mayer, G., Perez-Riverol, Y., Reisinger, F., Ternent, T. et al. (2016). 2016 update of the PRIDE database and its related tools. *Nucleic Acids Res.* 44, D447-D456.

Yang, D., Rismanchi, N., Renvoise, B., Lippincott-Schwartz, J., Blackstone, C. and Hurley, J. H. (2008). Structural basis for midbody targeting of spastin by the ESCRT-III protein CHMP1B. *Nat. Struct. Mol. Biol.* 15, 1278-1286.

Zhang, X. D., Goeres, J., Zhang, H., Yen, T. J., Porter, A. C. and Matunis, M. J. (2008). SUMO-2/3 modification and binding regulate the association of CENP-E with kinetochores and progression through mitosis. *Mol. Cell* 29, 729-741.

Zhou, M. and Wang, Y. L. (2008). Distinct pathways for the early recruitment of myosin II and actin to the cytokinetic furrow. *Mol. Biol. Cell* 19, 318-326.

Zhu, C., Lau, E., Schwarzenbacher, R., Bossy-Wetzel, E. and Jiang, W. (2006) Spatioteporal control of spindle midzone formation by PRC1 in human cells. *Proc. Natl. Acad. Sci. U S A* 103, 6196-6201.

Zhu, C. and Jiang, W. (2005) Cell cycle-dependent translocation of PRC1 on the spindle by Kif4 is essential for midzone formation and cytokinesis. *Proc. Natl. Acad. Sci. U S A* 102, 343-348.

Figures

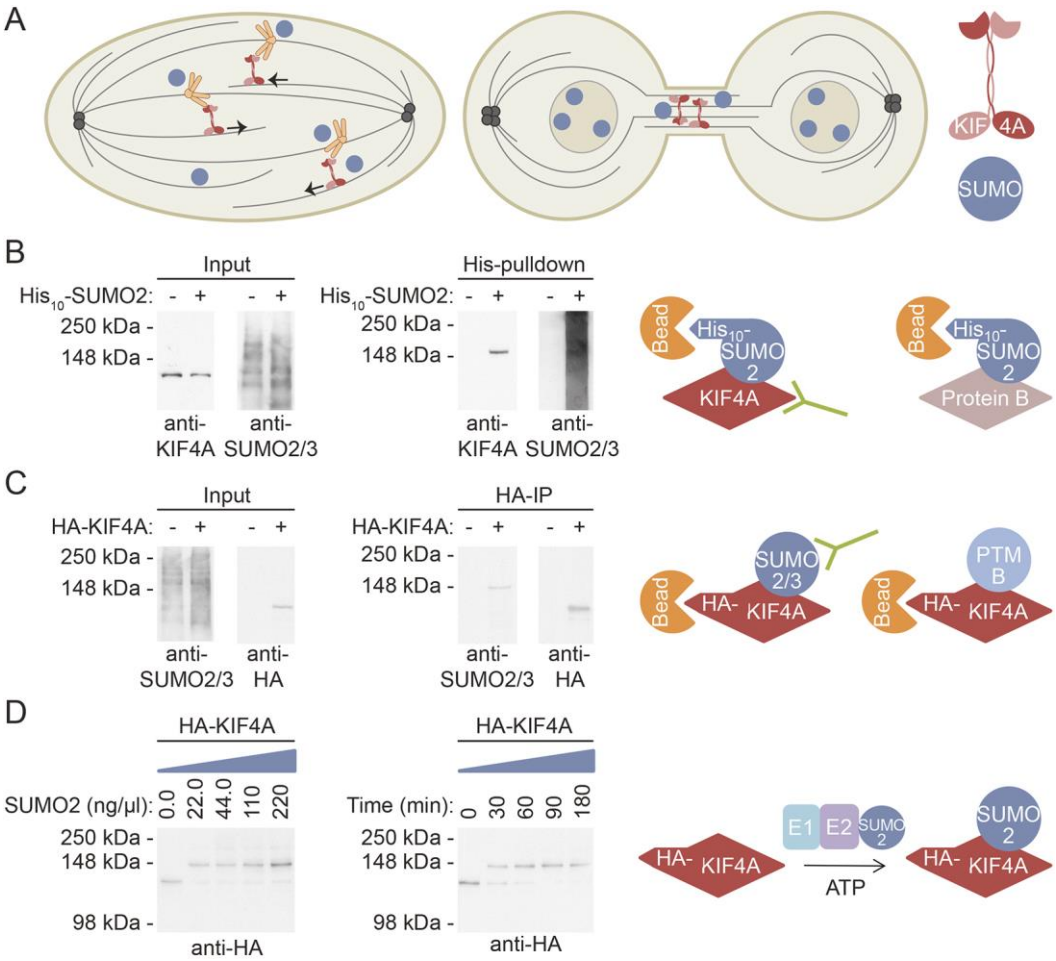

Fig. 1 The human chromokinesin KIF4A is modified by a single SUMO moiety. (**A**) Chromokinesin KIF4A is required for the positioning of mitotic chromosomes and stabilization of the bipolar spindle. In cytokinesis, KIF4A localizes at the intercellular bridge. The post-translational modifier SUMO is required for mitosis, and is conjugated to KIF4A. In this project, we investigate the functional role of KIF4A SUMOylation. (**B**) U2OS cells without or with stable expression of His_{10}-SUMO2 were lysed. A His_{10}-pulldown was performed to enrich for SUMOylated proteins. Input and pulldown samples were analyzed by immunoblotting using antibodies against KIF4A and SUMO2/3. The experimental procedure is summarized in the cartoon. (**C**) U2OS cells were transfected with a control or HA-KIF4A wildtype (WT) construct and lysed after three days. An HA-IP was performed to enrich HA-KIF4A WT. Input and IP samples were analyzed by immunoblotting using antibodies against SUMO2/3 or the HA-tag.

The cartoon illustrates the experimental procedure. (**D**) U2OS cells were transfected with a construct encoding HA-KIF4A WT, lysed after three days and an HA-IP was performed. The purified HA-KIF4A WT was *in vitro* SUMOylated by the addition of SUMO E1 and SUMO E2, either incubated at 4°C for three hours with the indicated concentrations of SUMO2 (left) or for the indicated time with 220 ng/µl SUMO2 (right). Samples were analyzed by immunoblotting using an antibody against the HA-tag. The cartoon summarizes the experimental procedure. Each experiment was performed at least three times.

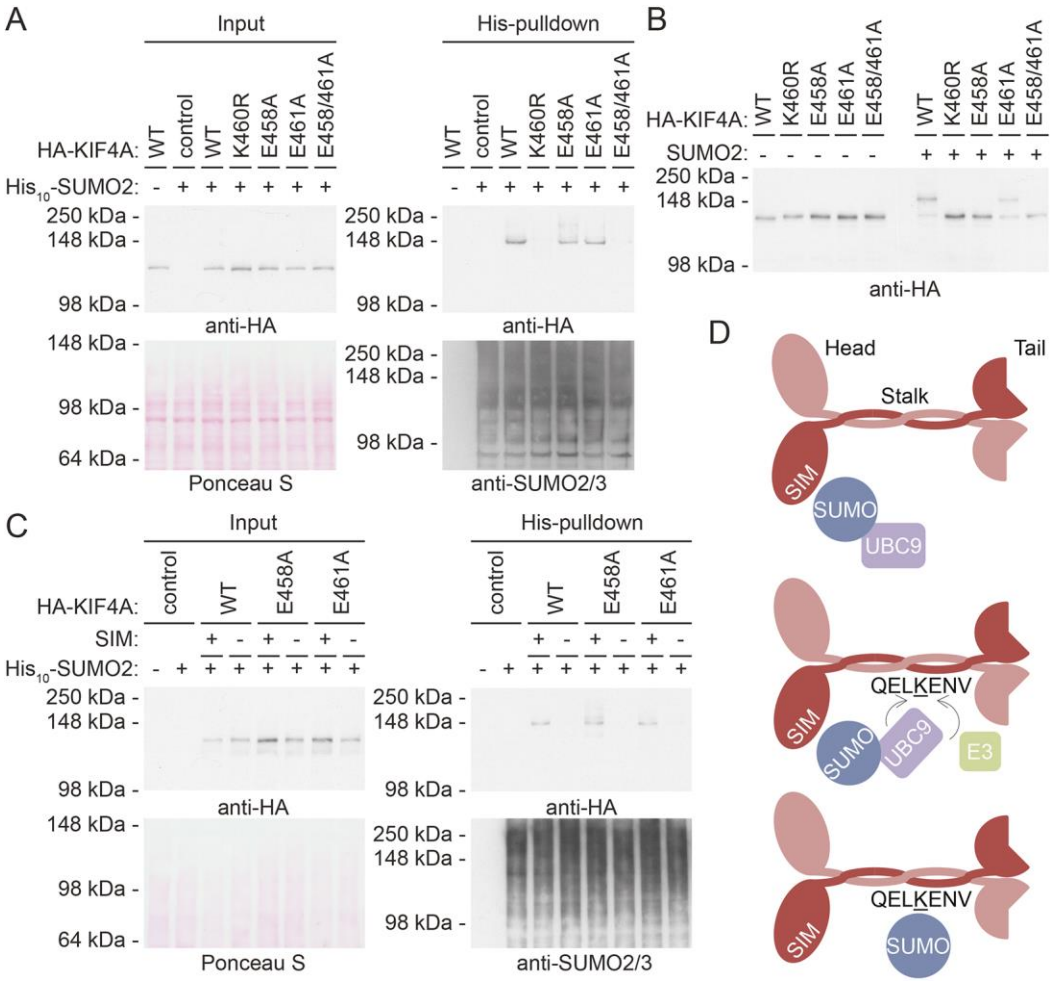

Fig. 2 KIF4A is SUMOylated on lysine 460 in a SIM dependent manner. (**A**) U2OS cells without or with stable expression of His_{10}-SUMO2 were transfected with a control, HA-KIF4A wildtype (WT) or indicated mutant construct and lysed after three days. A His_{10}-pulldown was performed to enrich for SUMOylated proteins. The samples were analyzed by immunoblotting using antibodies against the HA-tag and SUMO2/3, while equal loading was confirmed by Ponceau S staining. (**B**) U2OS cells were transfected with plasmids encoding HA-KIF4A WT or the indicated mutants, lysed after three days and the HA-tagged proteins were enriched by IP. An *in vitro* SUMOylation assay was performed by the addition of SUMO E1 and SUMO E2, followed by incubation for 3 hours at 4°C in the presence of 220 ng/µl SUMO2. Samples were analyzed by immunoblotting using an antibody against the HA-tag. (**C**) U2OS cells without or with stable expression of His_{10}-SUMO2 were transfected with control plasmid, or plasmids encoding HA-KIF4A WT, HA-KIF4A E458A or HA-KIF4A E461A that either did not or did

contain additional mutations to abolish the SUMO interaction motif (SIM ILDLL mutated to AADAA). After three days, cells were lysed. Upon enrichment for SUMOylated proteins by His_{10}-pulldown, samples were analyzed by immunoblotting with antibodies against the HA-tag or SUMO2/3 and by Ponceau S staining to confirm equal loading. Each experiment was performed at least three times. (**D**) A cartoon depicting the proposed mechanism of KIF4A SUMOylation in human cells. The SUMO E2 (UBC9)-SUMO complex interacts with the KIF4A dimer via the SIM in its head domain. Subsequently, UBC9 is able to covalently attach SUMO to lysine 460 in the stalk domain, either directly through the inverted consensus motif (ExK) or with the help of a SUMO E3 ligase through the second motif (KE).

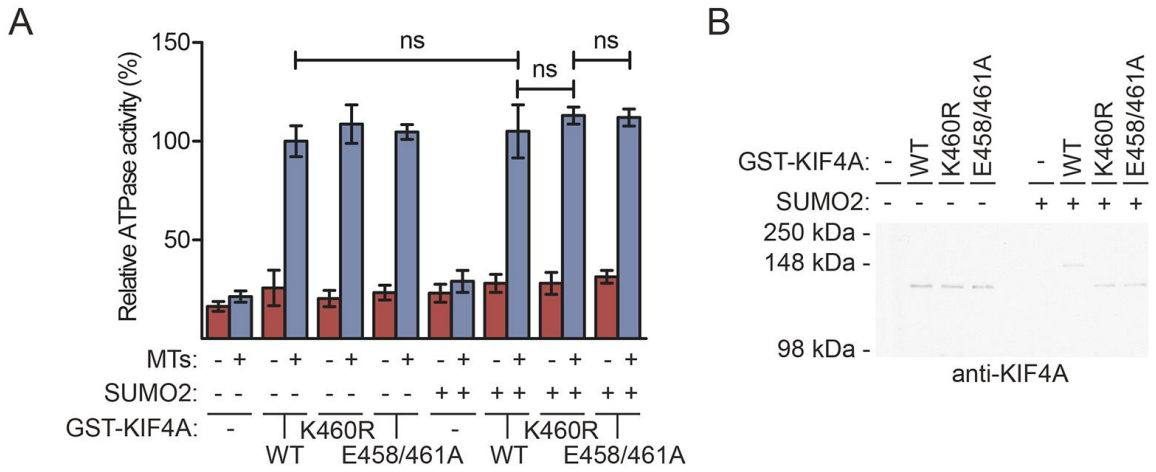

Fig. 3 SUMOylation does not affect ATPase activity of KIF4A. (**A**) *In vitro* SUMOylation reactions were performed on negative control samples and samples containing wildtype (WT) or SUMOylation deficient (K460R and E458/461A) recombinant GST-KIF4A. Additional negative control assays were carried out in the absence of SUMO2 as indicated. Subsequently, an ATPase activity assay was performed in the absence or presence of microtubules (MTs) and absorbance was measured. The mean percentage of relative ATPase activity for three independent experiments is shown and standard deviations are provided. A two-sided Student T-test was used to calculate p values and the difference was considered not significant (ns) when $p > 0.05$. (**B**) Aliquots of the *in vitro* SUMOylation samples, used for the experiment described in Figure 3A, were used to verify SUMOylation efficiency by immunoblotting with an antibody against KIF4A.

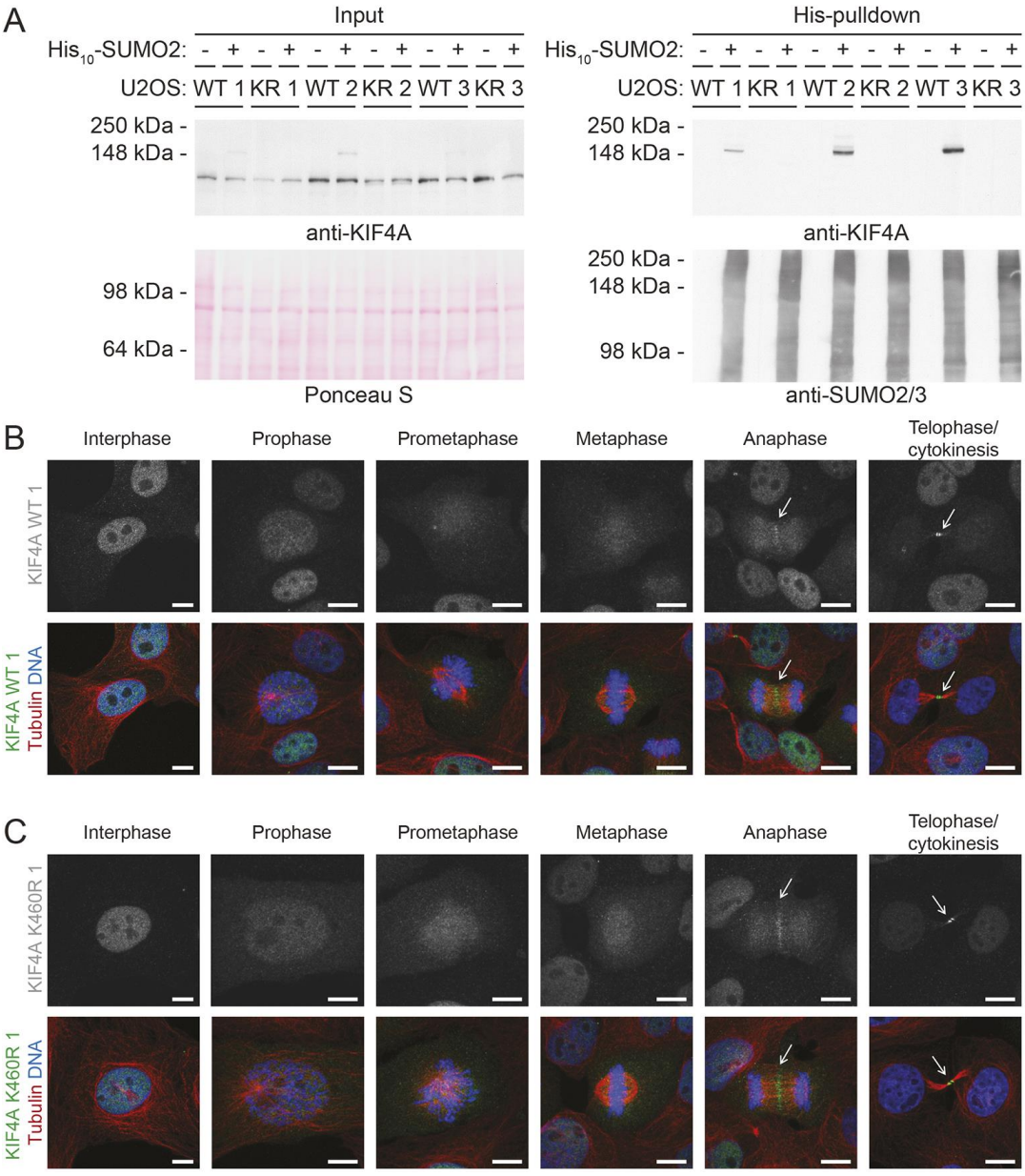

Fig. 4 The localization of endogenous KIF4A during mitosis is not dependent on SUMOylation. (**A**) Three KIF4A mutant (K460R) clones and their KIF4A wildtype (WT) control clones obtained by CRISPR-Cas9-directed genome editing were infected with lentivirus encoding His_{10}-SUMO2 and selected with puromycin to obtain stable cell lines. Subsequently, these cells were lysed. A His_{10}-pulldown was performed to enrich for SUMOylated proteins. Input and pulldown samples were analyzed by immunoblotting using antibodies against KIF4A and SUMO2/3, while Ponceau S staining was used to confirm equal loading. (**B**) U2OS clone 1 with endogenous wildtype KIF4A (WT) or (**C**) with endogenous SUMOylation deficient KIF4A

(K460R) were grown on glass slides, fixed and stained with antibodies against KIF4A (green), tubulin (red) and Hoechst to visualize DNA (blue). Representative images were taken of cells in subsequent stages of mitosis to visualize KIF4A localization. Scale bars correspond to 10 µm. Each experiment was performed at least three times.

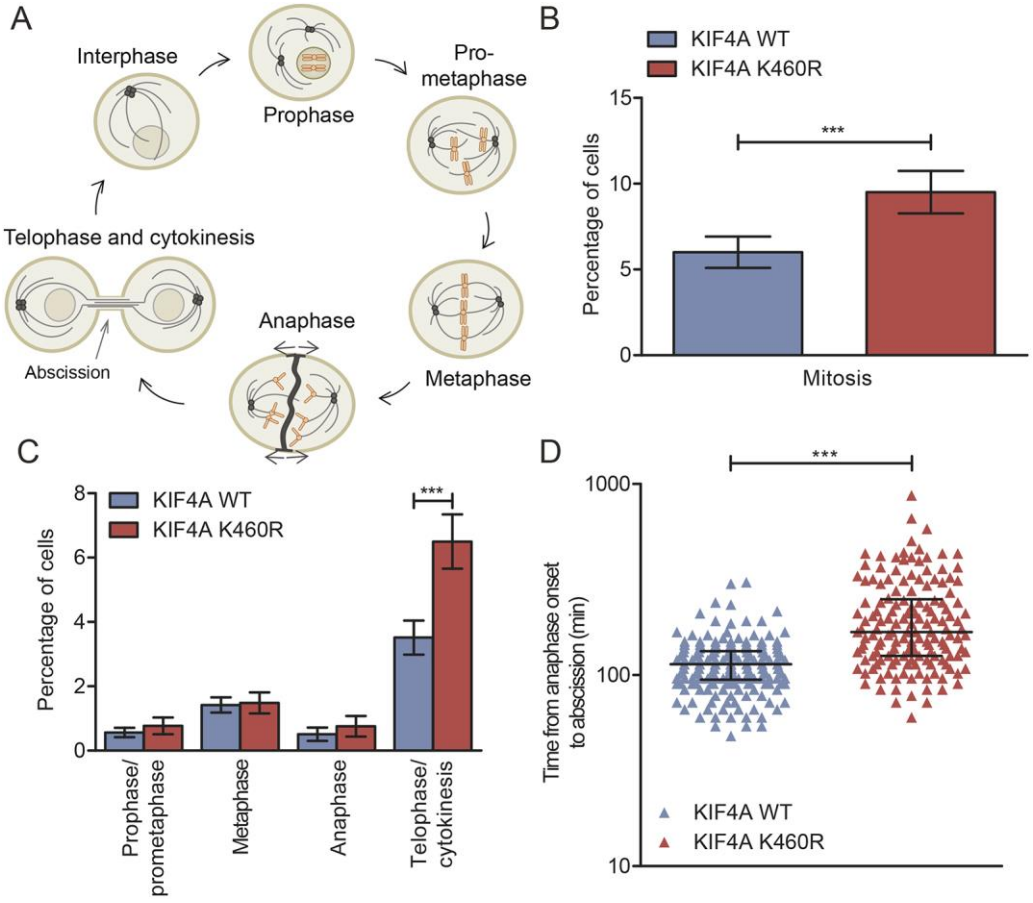

Fig. 5 SUMOylation of endogenous KIF4A regulates abscission. (**A**) Cartoon depicting the subsequent phases of mitosis during cell division. (**B**) Three independent sets consisting of a KIF4A WT and K460R clone were fixed and stained as described in Figure 4B and 4C. Random images were taken and the total amount of cells and the number of cells in mitosis per field were analyzed for at least 400 cells per clone per experiment. The percentage of cells in mitosis was averaged for the three WT and the three K460R KIF4A clones. Mean values with standard deviations are shown. The p value was calculated using a two-sided Student T-test and three stars represent $p < 0.0005$. (**C**) The mitotic cells identified in the experiment described in Figure 5B were categorized into prophase/prometaphase, metaphase, anaphase or telophase/cytokinesis. The percentage of cells in each phase of mitosis was averaged for the three WT and the three K460R clones. Mean values and standard deviations are shown. P values were calculated using a two-sided Student T-test and three stars represent $p < 0.0005$. Each experiment was performed at least three times. (**D**) All three WT and three

K460R KIF4A clones were transfected with a GFP-tubulin construct, selected using G418, subcloned and sorted by flow cytometry to obtain stable cell lines with equal GFP-tubulin expression. Live cell imaging was used to analyze the time from anaphase onset to abscission, based on the DIC and GFP-tubulin signal for 66 cells per WT clone and 51 cells per K460R clone. The data obtained from the individual WT as well as the individual K460R clones were pooled and each cell is represented by a colored triangle. Median values with interquartile ranges are shown in black. The p value was calculated using a Mann Whitney test and three stars represent $p < 0.0005$.

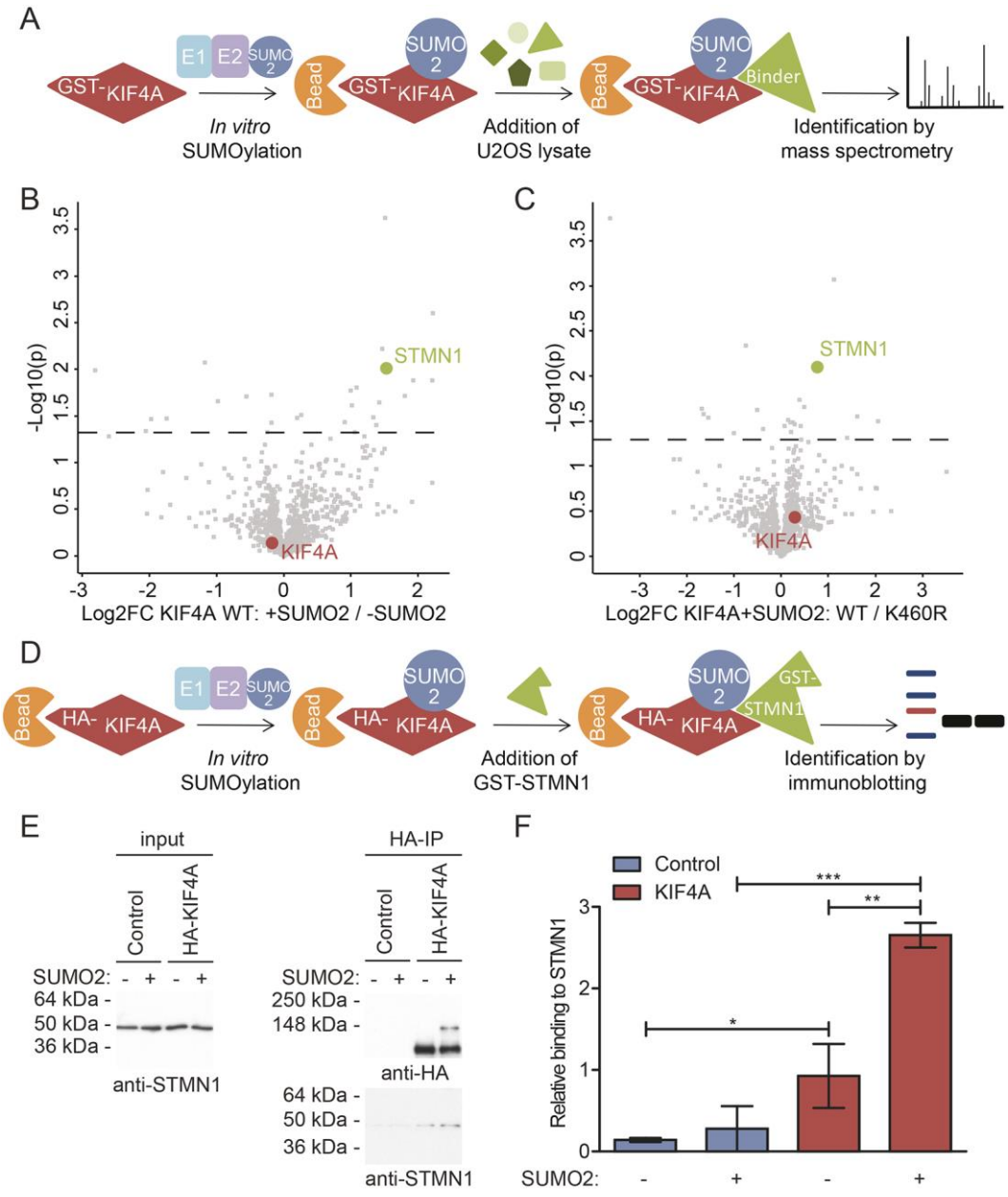

Fig. 6 SUMOylation of KIF4A enhances binding to STMN1. (**A**) A cartoon depicting the experimental set-up to identify proteins binding preferentially to SUMOylated KIF4A. Recombinant GST-KIF4A wildtype (WT) or SUMOylation deficient mutant (K460R) were bound to beads and *in vitro* SUMOylation assays were performed. In control assays, SUMO2 was omitted. Subsequently, U2OS cell lysates were added, incubation was performed, samples were washed and bound proteins were identified by mass spectrometry. (**B**) Volcano plot showing proteins binding preferentially to SUMOylated over non-SUMOylated GST-KIF4A. On the x-axis, the Log2 fold change (FC) between the proteins identified by mass

spectrometry in the samples bound to SUMOylated GST-KIF4A WT versus non-SUMOylated GST-KIF4A WT is indicated. On the y-axis the -Log10(p) values for the identified proteins are shown. All proteins above the dashed line were considered significant ($p < 0.05$). (**C**) Volcano plot showing proteins binding preferentially to SUMOylated GST-KIF4A WT over the K460R mutant. The Log2FC and -Log10(p) values for the identified proteins are shown. Proteins above the dashed line were considered significant ($p < 0.05$). (**D**) Cartoon depicting the experimental procedure employed to verify STMN1 as a differential binder identified by mass spectrometry. U2OS cells were transfected with a control or HA-KIF4A WT construct and lysed after three days. Upon purification via HA-IP, an *in vitro* SUMOylation assay was performed and in the negative control SUMO2 was omitted. Finally, the samples were incubated with recombinant GST-STMN1, washed extensively and eluted. (**E**) Input and IP samples from the experiment described above were analyzed by immunoblotting using antibodies against the HA-tag and STMN1. (**F**) Quantification of the result of three independent experiments as presented in Figure 6E. The mean relative binding of GST-STMN1 to KIF4A is shown with standard deviations. A two-sided Student T-test was used to calculate p values. One star represents $p < 0.05$, two stars $p < 0.005$ and three stars $p < 0.0005$. Each experiment was performed at least three times.

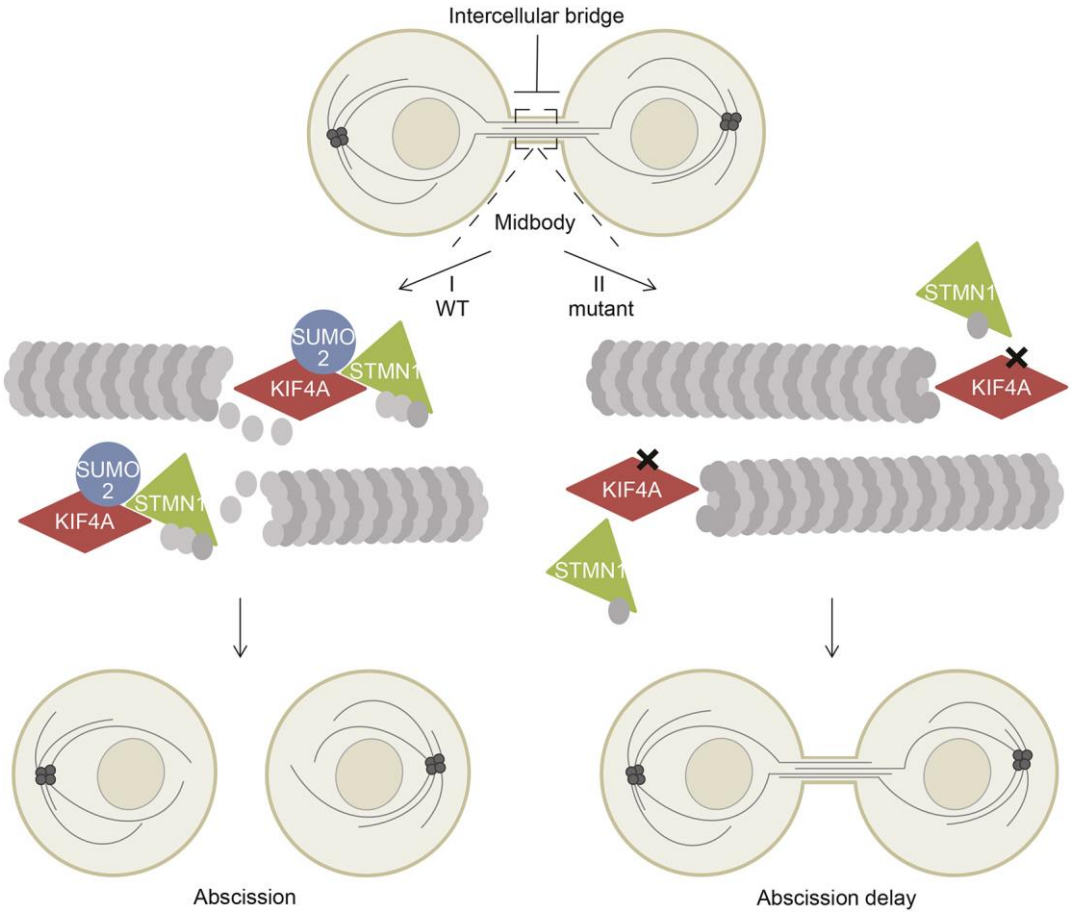

Fig. 7 Model: SUMOylation of KIF4A enhances binding to microtubule destabilizer STMN1 and promotes abscission. Cartoon depicting the intercellular bridge between the newly formed daughter cells during cytokinesis. (**I**) In cells expressing wildtype KIF4A, SUMOylation of KIF4A enhances its binding to STMN1 at the midbody. Subsequently, microtubule destabilization by STMN1 is promoted, which results in abscission and thereby completes the final step of cell division. (**II**) Blocking KIF4A SUMOylation reduces STMN1 binding. Consequently, this results in reduced microtubule destabilization by STMN1 at the midbody and ensuing delay in abscission.

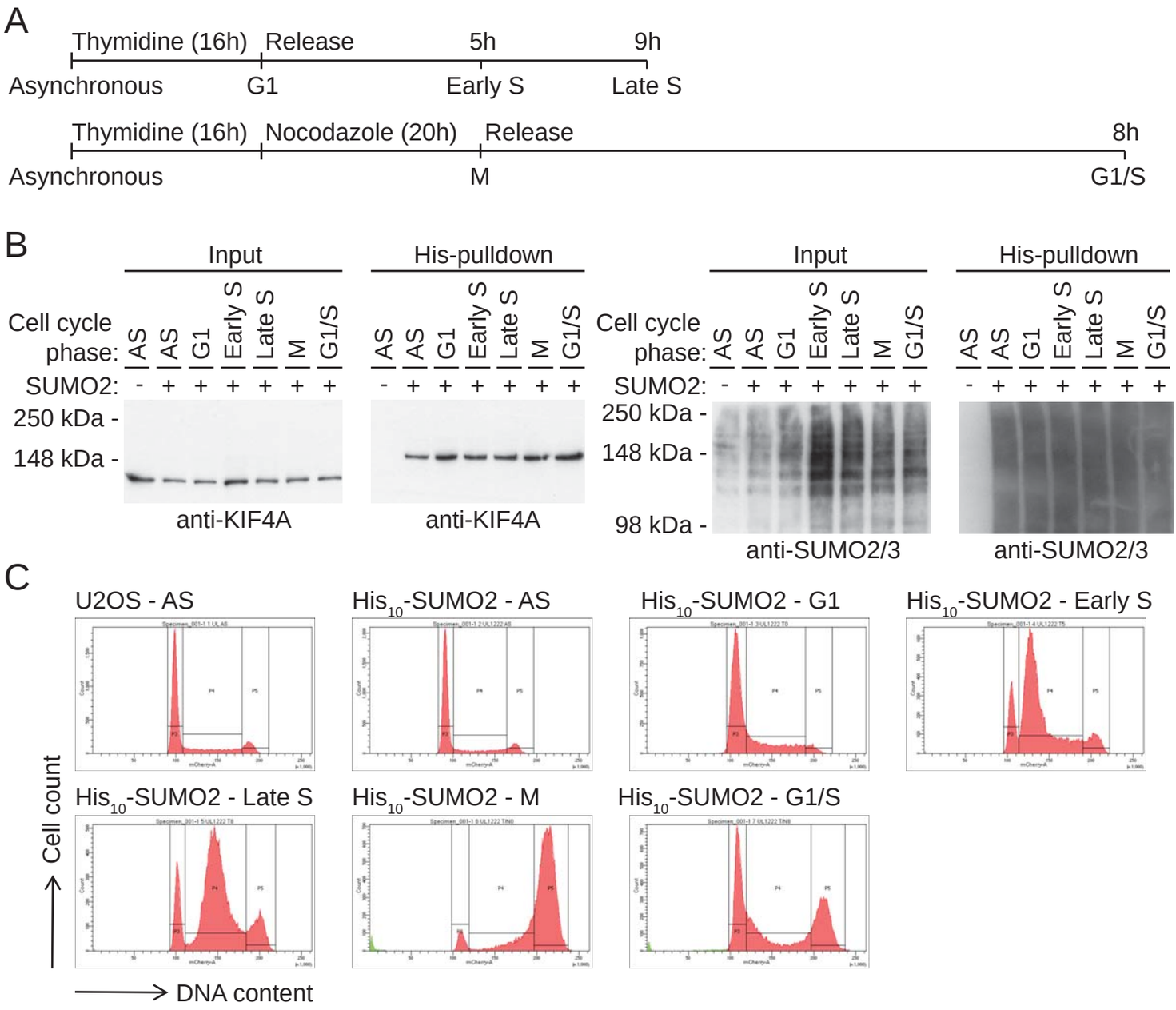

Figure S1 SUMOylation of endogenous KIF4A is stable during cell cycle progression. (**A**) Overview of the cell cycle synchronization strategy indicates the treatment, time of incubation and time of release to obtain cells in the indicated cell cycle phase. (**B**) U2OS cells without or with stable expression of his_{10}-SUMO2 were synchronized at the indicated cell cycle phases using thymidine and nocodazole. Cells were lysed and his_{10}-pulldowns were performed to enrich for SUMOylated proteins. Samples were analyzed by immunoblotting using antibodies against KIF4A and SUMO2/3. (**C**) Cell cycle synchronization described in Supplementary information, Figure 1B was confirmed by flow cytometry. Each experiment was performed at least three times.

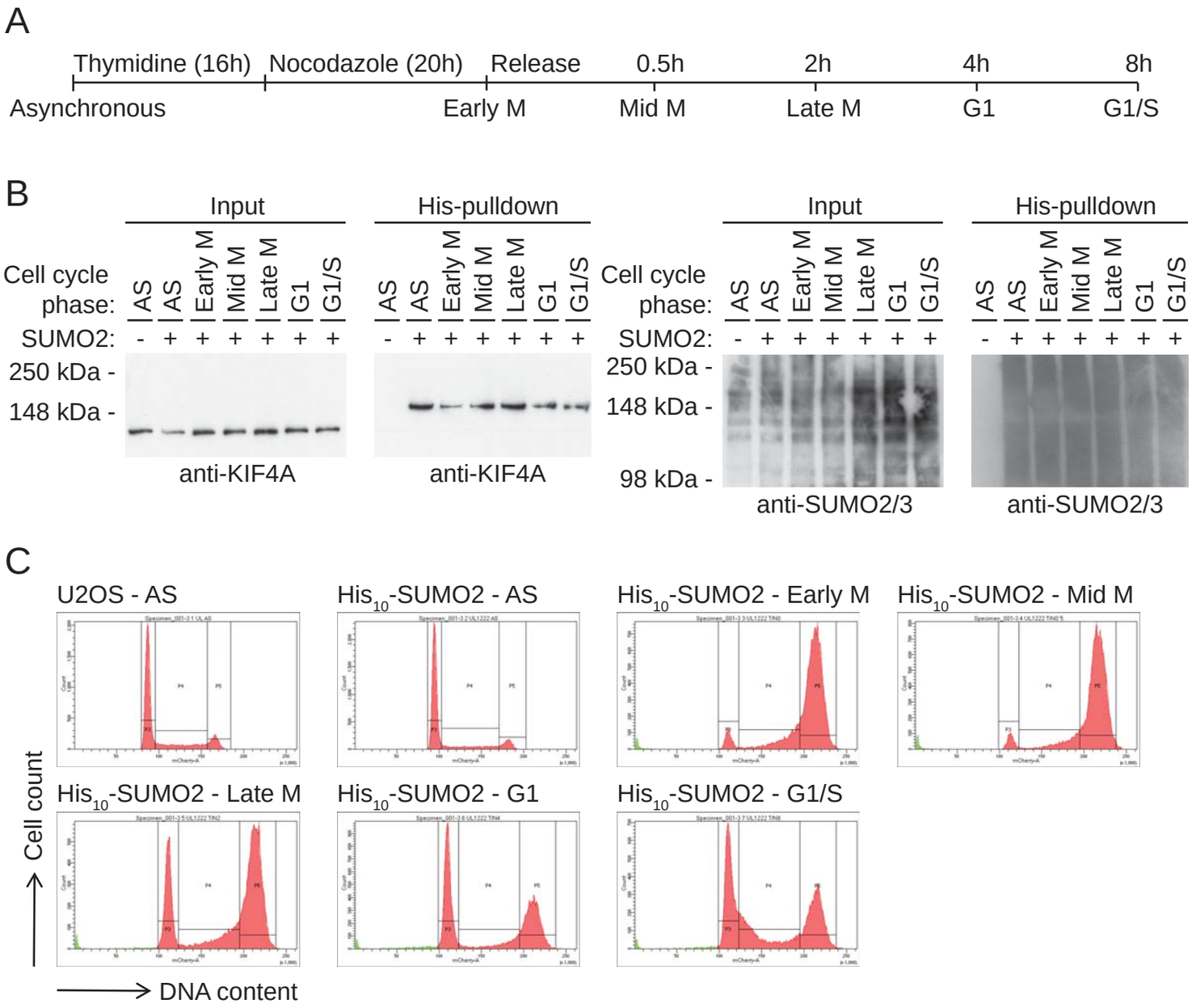

Figure S2 SUMOylation of endogenous KIF4A is stable during mitotic progression. (**A**) Overview of the cell cycle synchronization strategy indicates the treatment, time of incubation and time of release to obtain cells in the indicated mitotic phase. (**B**) U2OS cells without or with stable expression of his_{10}-SUMO2 were synchronized in mitosis as indicated using thymidine and nocodazole. Cells were lysed and his_{10}-pulldowns were performed to enrich for SUMOylated proteins. Input and pulldown samples were analyzed by immunoblotting using antibodies against KIF4A and SUMO2/3. (**C**) Mitotic cell cycle synchronization described in Supplementary information, Figure 2B was confirmed by flow cytometry. Each experiment was performed at least three times.

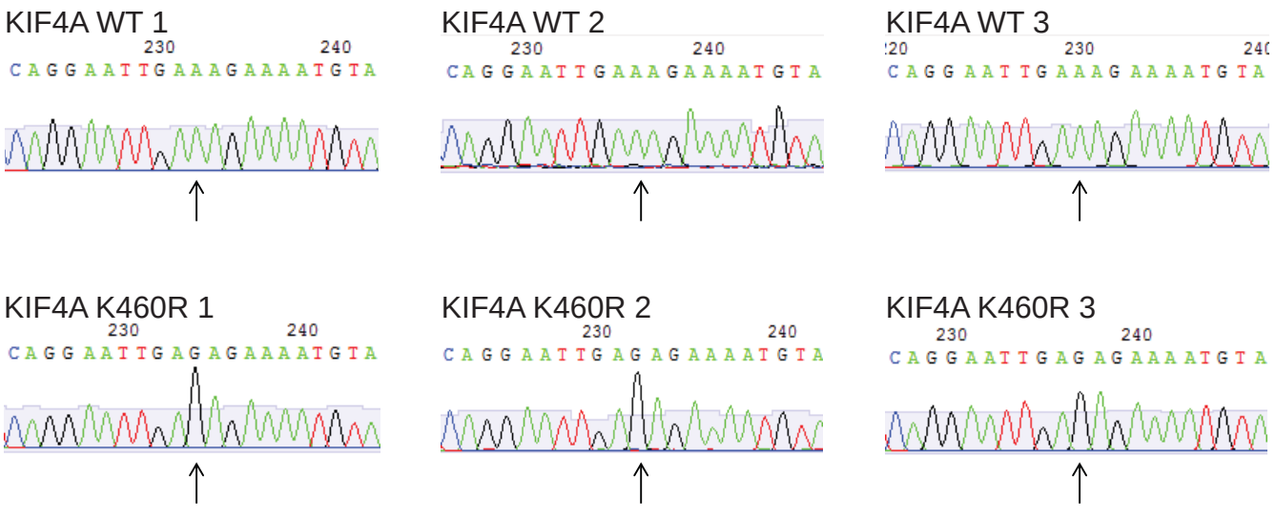

Figure S3 CRISPR-Cas9-directed genome editing was used in combination with a repair template for targeted mutation of the KIF4A gene, resulting in a replacement of the endogenous lysine 460 with an arginine in the KIF4A protein. After subcloning, genome editing was verified by PCR amplification and diagnostic digestion. Subsequently, sequencing was performed to confirm either wildtype (WT) or mutant (K460R) KIF4A identity.

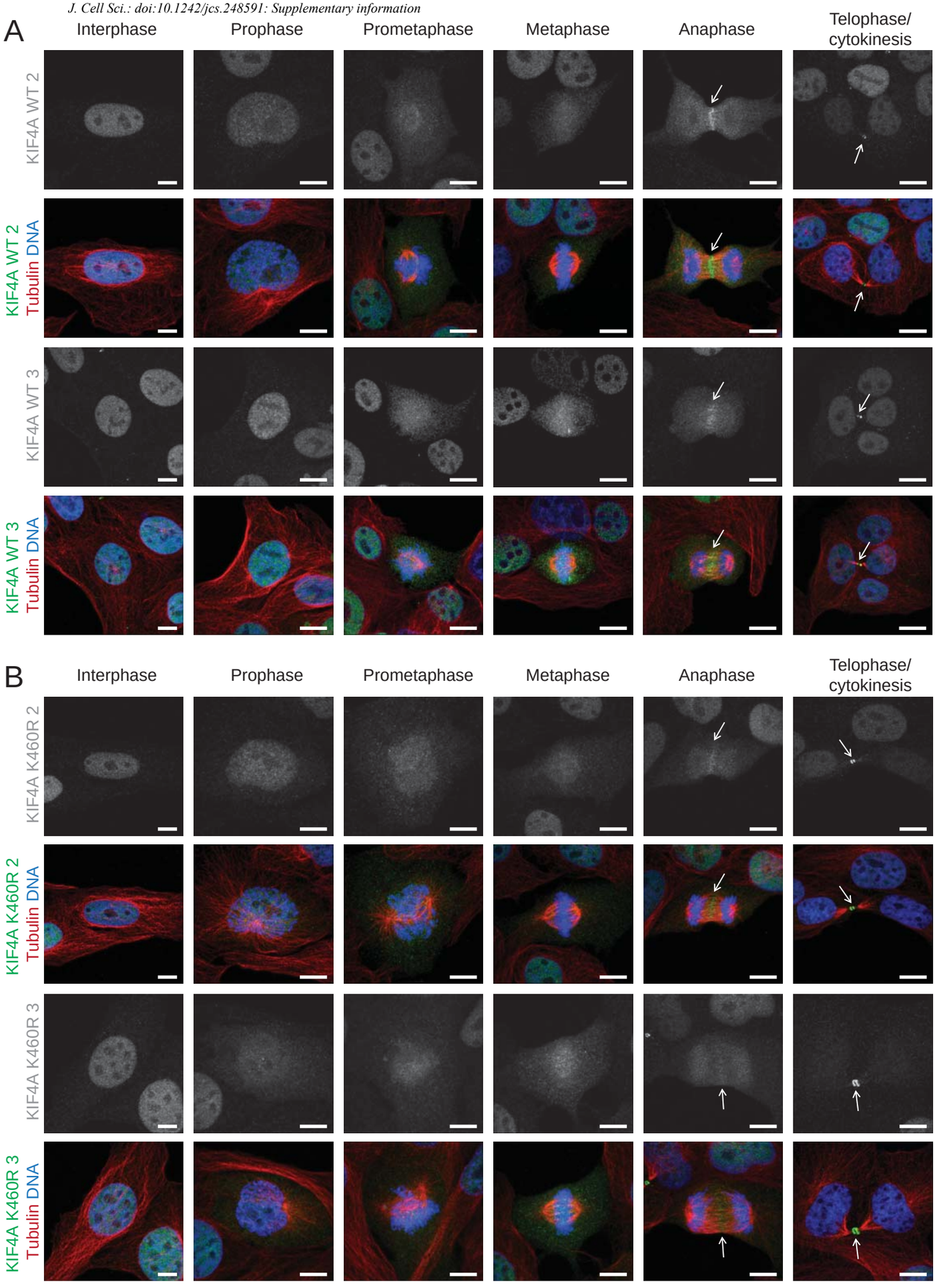

Figure S4 The localization of endogenous KIF4A during mitosis is not dependent on SUMOylation. (**A**) Two additional U2OS cell lines expressing endogenous WT KIF4A (clone 2 and 3) or (**B**) endogenous K460R KIF4A (clone 2 and 3) were grown on glass slides, fixed and stained with antibodies against KIF4A (green), tubulin (red) and Hoechst to visualize DNA (blue). Representative images were taken of cells in different stages of mitosis to visualize KIF4A localization. Scale bars correspond to 10 μm. Each experiment was performed at least three times.

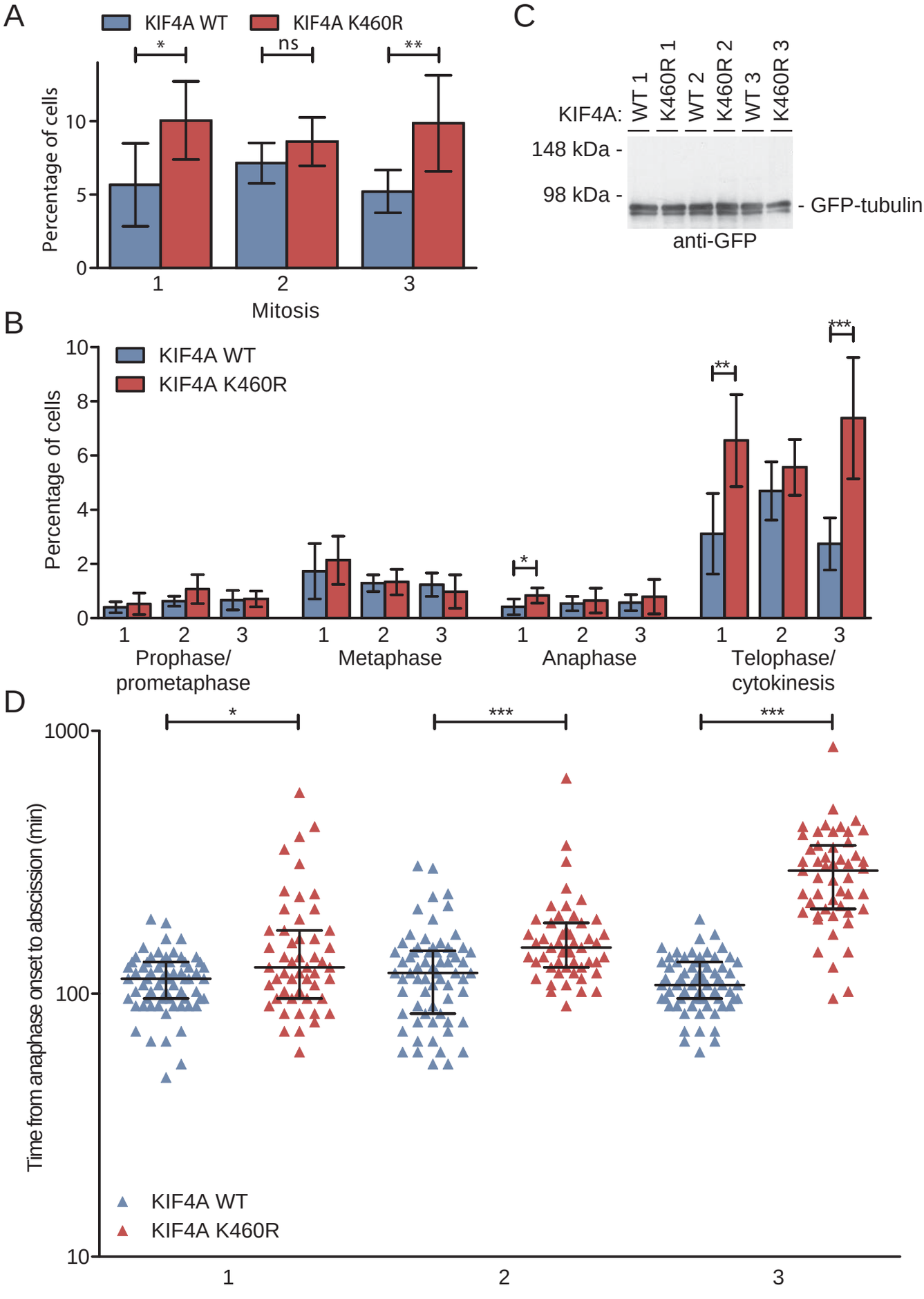

Figure S5 Increased mitotic index and delay in abscission in cells deficient for SUMOylation of endogenous KIF4A. (**A**) Three independent sets (1, 2 and 3) of KIF4A wildtype (WT) and SUMOylation deficient (K460R) clones were fixed and stained with Hoechst and antibodies directed against KIF4A and tubulin. Images were taken randomly and analyzed for the total amount of cells and the number of cells in mitosis. The mean percentage of cells in mitosis for each set of KIF4A WT and K460R clones is shown with corresponding standard deviations. P values were calculated using a two-sided Student T-test. One star represents $p < 0.05$ and two stars $p < 0.005$. ns, not significant. (**B**) The mitotic cells identified in the experiment described in Supplementary information, Figure 5A were categorized into prophase/prometaphase, metaphase, anaphase or telophase/cytokinesis. The mean percentage of cells in each phase of mitosis for each set of KIF4A WT and K460R clones is shown with corresponding standard deviations. P values were calculated using a two-sided Student T-test. One star represents $p < 0.05$, two stars $p < 0.005$ and three stars $p < 0.0005$. Each experiment was performed at least three times. (**C**) All three WT and three K460R KIF4A clones were transfected with a GFP-tubulin construct, selected using G418, subcloned and sorted by flow cytometry to obtain stable cell lines with equal GFP-tubulin expression. Cells were lysed and samples were analyzed by immunoblotting using an antibody against GFP. (**D**) Live cell imaging was used to analyze the time from anaphase onset to abscission, based on the DIC and GFP-tubulin signal for 66 cells per WT clone and 51 cells per K460R clone. Each individual cell is represented by a colored triangle, while the medians with interquartile ranges are shown in black for each set of WT and K460R clone. P values were calculated using the Mann Whitney test. One star represents $p < 0.05$ and three stars $p < 0.0005$.

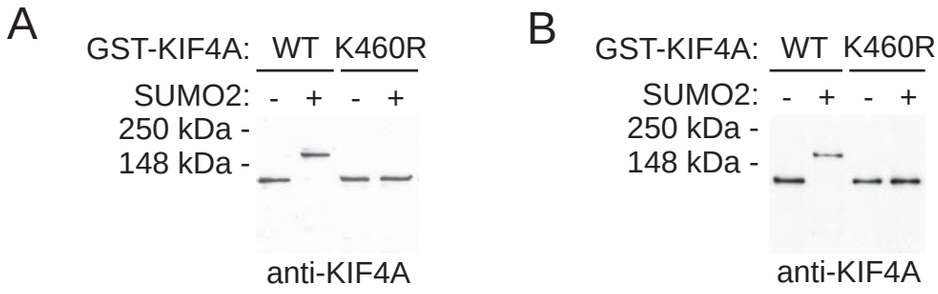

Figure S6 Confirmation of *in vitro* SUMOylation KIF4A before and after lysate incubation. (**A**) Recombinant GST-KIF4A wildtype (WT) or SUMOylation deficient mutant (K460R) were bound to beads and an *in vitro* SUMOylation assay was performed in the absence or presence of SUMO2. Aliquots of the samples were used to verify SUMOylation efficiency by immunoblotting using an antibody against KIF4A. (**B**) The samples described in Supplementary information, Figure 6A were incubated with a U2OS lysate and washed. Prior to sample preparation for mass spectrometry analysis, aliquots of the samples were saved to verify SUMOylation and protein levels by immunoblotting using an antibody against KIF4A. Each experiment was performed at least three times.

A

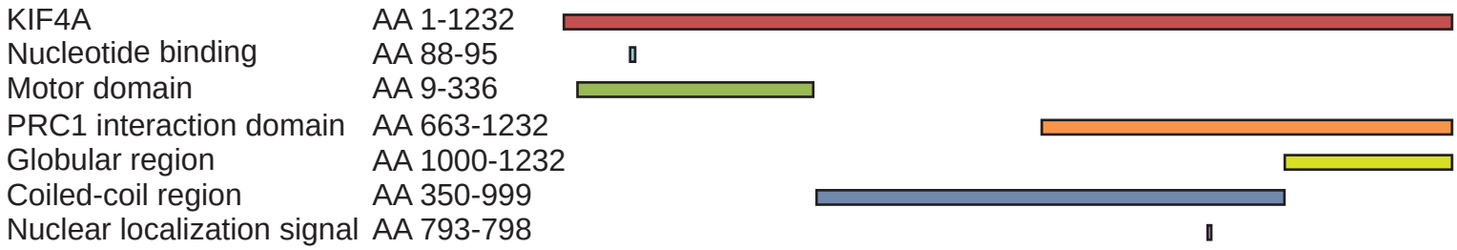

B

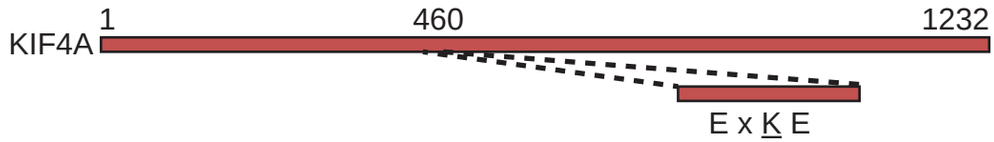

Homo sapiens	428	EKMNAKLEELRQ-------HAACKLDL-QKLVETLEDQELKENVEIICNL	469
Canis lupus familiaris	429	EKMNAKLEELRQ-------HAALKVDL-QKLVETLEDQELKENVEIIRNL	470
Bos taurus	429	EKMNAKLEELRK-------HAACKVDL-QKLVETLEDQELKENVEIIRNL	470
Mus musculus	429	EKMNAKLEELRR-------HAACKVDL-QKLVETLEDQELKENIEIICNL	470
Rattus norvegicus	429	EKMNAKLEELRQ-------HAACKVDL-QKLAETLEDQEVKENIEIICNL	470
Gallus gallus	431	EKMNAKLEQLQQ-------HAVCKLDL-QKLLETVEDEELKENVEVIRNL	472
Xenopus (Silurana) tropicalis	429	EKLASKIEELKQ-------HAACKVDL-QRLVETLEDQELKENVGVILDL	470
Drosophila melanogaster	445	DKLRSHVSELKN-------KLDQREQAQFGNENTNGDNEMRDFSLLVNRV	487
Caenorhabditis elegans	416	SRLEEDKAKLQS--------------MLTDVRNTVLNEEMLDAAEVVRSI	451
Arabidopsis thaliana	445	DKLIMIIESVRNGKSLDEIESCQNEDVGLVNKYVSKIQELEGELLHIKNL	494

C

Homo sapiens	139	SYLEIYNEEILDLLCPSRE--------------K--A-QINIREDPKEGI	171
Canis lupus familiaris	139	SYLEIYNEEILDLLCPSRE--------------K--ASQINIREDPKEGI	172
Bos taurus	139	SYLEIYNEEILDLLCPSRE--------------K--APQINIREDPKEGI	172
Mus musculus	139	SYLEIYNEEILDLLCSSRE--------------K--ATQINIREDPKEGI	172
Rattus norvegicus	139	SYLEIYNEEILDLLCSSRE--------------K--ASQINIREDPKEGI	172
Gallus gallus	139	SYLEIYNEDILDLLCSSRE--------------R--SSQISIREDPKEGI	172
Xenopus (Silurana) tropicalis	138	SYLEIYNEEILDLLYAARD--------------K--TNAISIREDPKEGI	171
Drosophila melanogaster	138	SFVELYQEQFYDLFSSKTR--------------D--KATVDIRE-VKNRI	170
Caenorhabditis elegans	136	SMFEVYGDNVYDLLRPDKV------------------KLNVHGDEKN-C	165
Arabidopsis thaliana	134	SFIEIFKEEVFDLLDSNSSALLKNDSGVQAKHTALSRAPIQIRETASGGI	183

Figure S7 KIF4A SUMOylation site and SUMO interaction motif conservation. (**A**) A cartoon depicting the localization of known domains and regions in the KIF4A protein. AA, amino acid. (**B**) Cartoon showing the localization of the SUMOylation site, containing lysine 460, in the KIF4A protein and the conservation of this region across the indicated species. (**C**) Cartoon depicting the localization of the SUMO interaction motif (SIM) in the KIF4A protein and the conservation of this region across the indicated species.

Table S1 Key of sample names. This sheet explains which sample name belongs to each exact sample measured.

Click here to Download Table S1

Table S2 A list of all peptides identified by Max Quant on the RAW Peptides sheet.

Click here to Download Table S2

Table S3 A list of all protein groups for which peptides were identified by Max Quant on the RAW ProteinGroups sheet.

Click here to Download Table S3

Table S4 A list of proteins for which their binding to KIF4A is significantly affected by SUMOylation. The line separates proteins that were identified to preferentially bind SUMOylated KIF4A (top) from the proteins that favoured binding to non-SUMOylated KIF4A (bottom).

Click here to Download Table S4

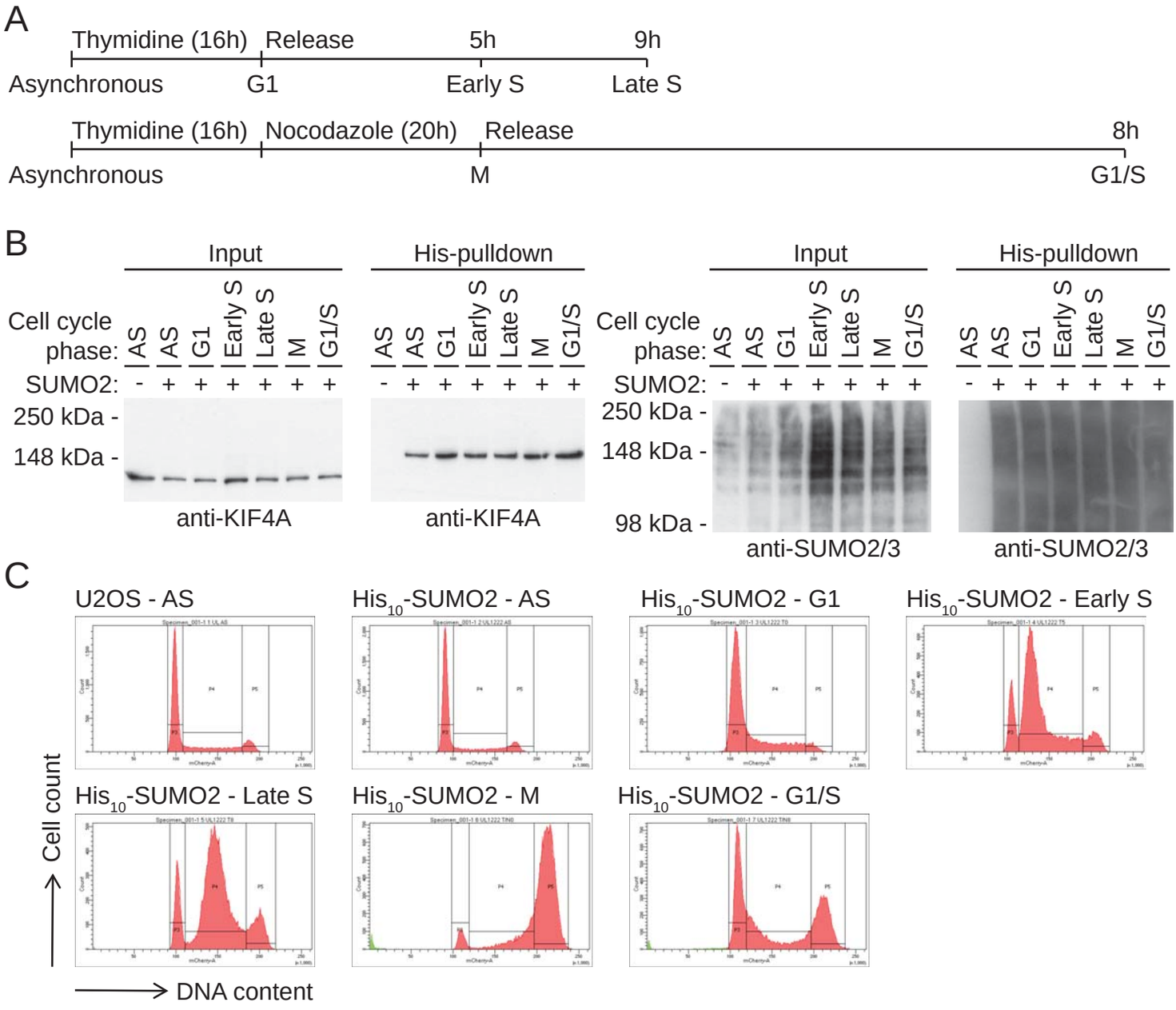

Figure S1 SUMOylation of endogenous KIF4A is stable during cell cycle progression. (**A**) Overview of the cell cycle synchronization strategy indicates the treatment, time of incubation and time of release to obtain cells in the indicated cell cycle phase. (**B**) U2OS cells without or with stable expression of his_{10}-SUMO2 were synchronized at the indicated cell cycle phases using thymidine and nocodazole. Cells were lysed and his_{10}-pulldowns were performed to enrich for SUMOylated proteins. Samples were analyzed by immunoblotting using antibodies against KIF4A and SUMO2/3. (**C**) Cell cycle synchronization described in Supplementary information, Figure 1B was confirmed by flow cytometry. Each experiment was performed at least three times.

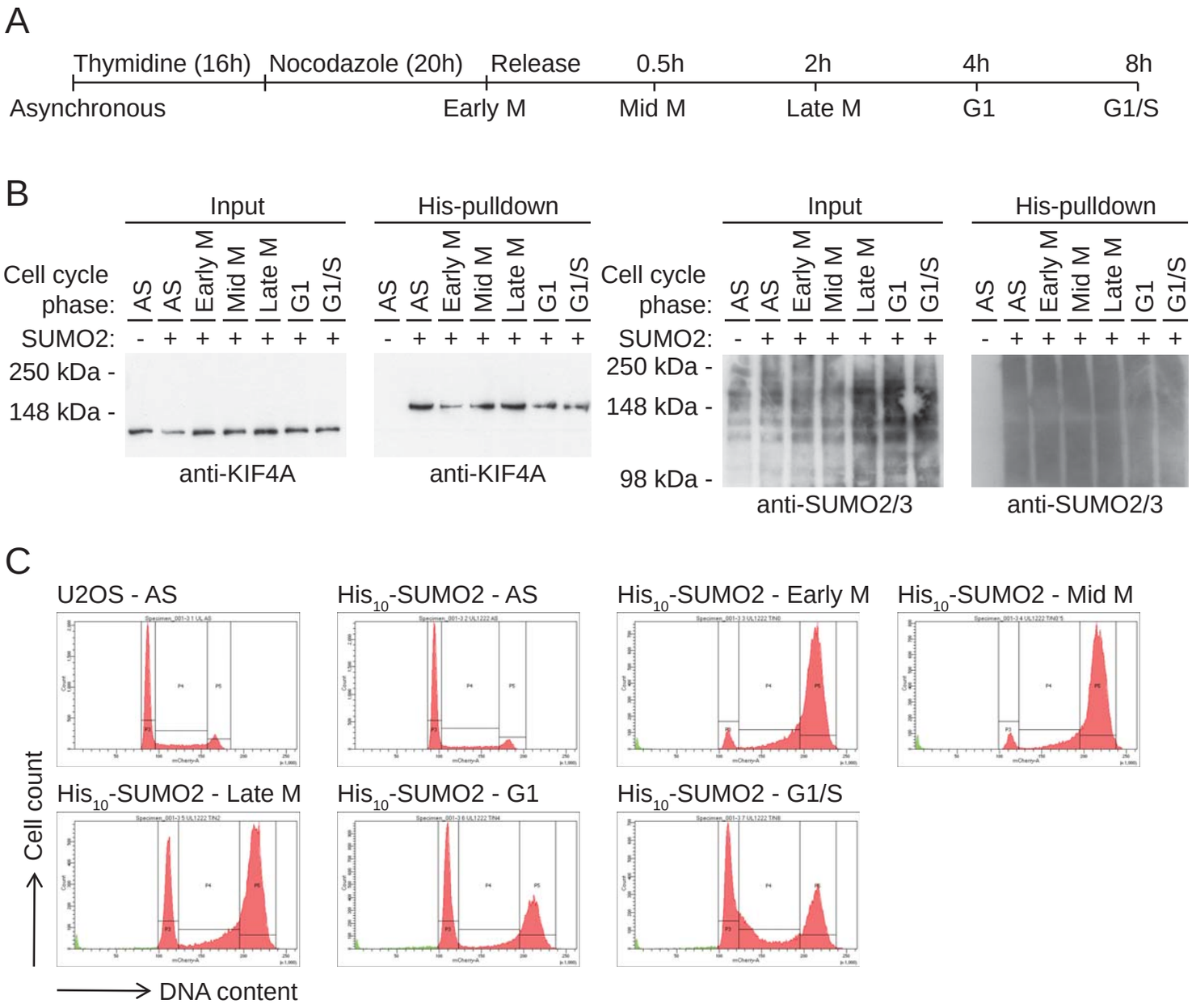

Figure S2 SUMOylation of endogenous KIF4A is stable during mitotic progression. (**A**) Overview of the cell cycle synchronization strategy indicates the treatment, time of incubation and time of release to obtain cells in the indicated mitotic phase. (**B**) U2OS cells without or with stable expression of his_{10}-SUMO2 were synchronized in mitosis as indicated using thymidine and nocodazole. Cells were lysed and his_{10}-pulldowns were performed to enrich for SUMOylated proteins. Input and pulldown samples were analyzed by immunoblotting using antibodies against KIF4A and SUMO2/3. (**C**) Mitotic cell cycle synchronization described in Supplementary information, Figure 2B was confirmed by flow cytometry. Each experiment was performed at least three times.

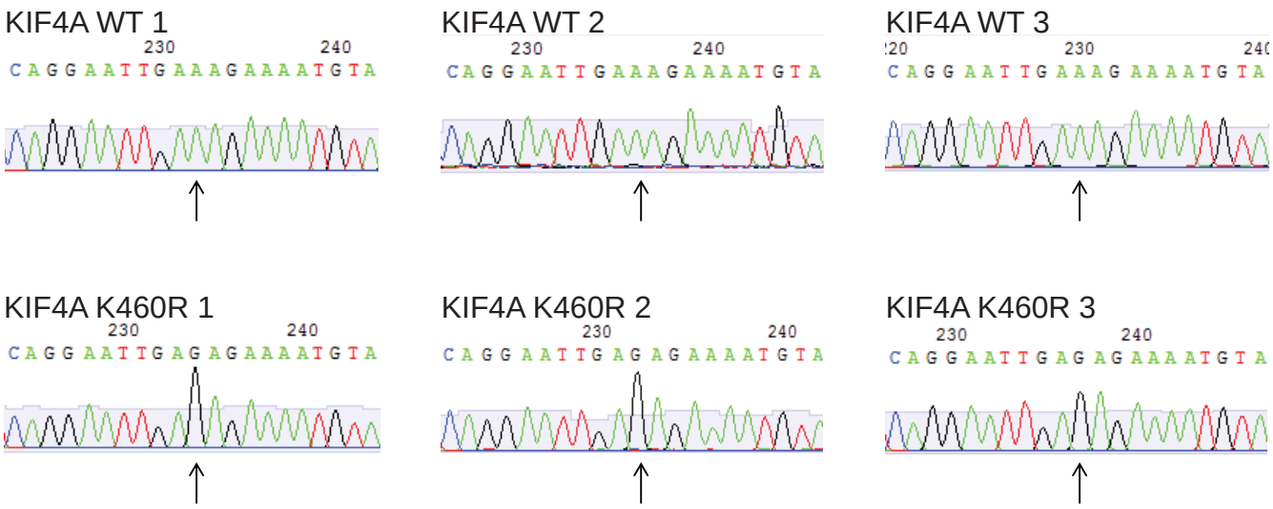

Figure S3 CRISPR-Cas9-directed genome editing was used in combination with a repair template for targeted mutation of the KIF4A gene, resulting in a replacement of the endogenous lysine 460 with an arginine in the KIF4A protein. After subcloning, genome editing was verified by PCR amplification and diagnostic digestion. Subsequently, sequencing was performed to confirm either wildtype (WT) or mutant (K460R) KIF4A identity.

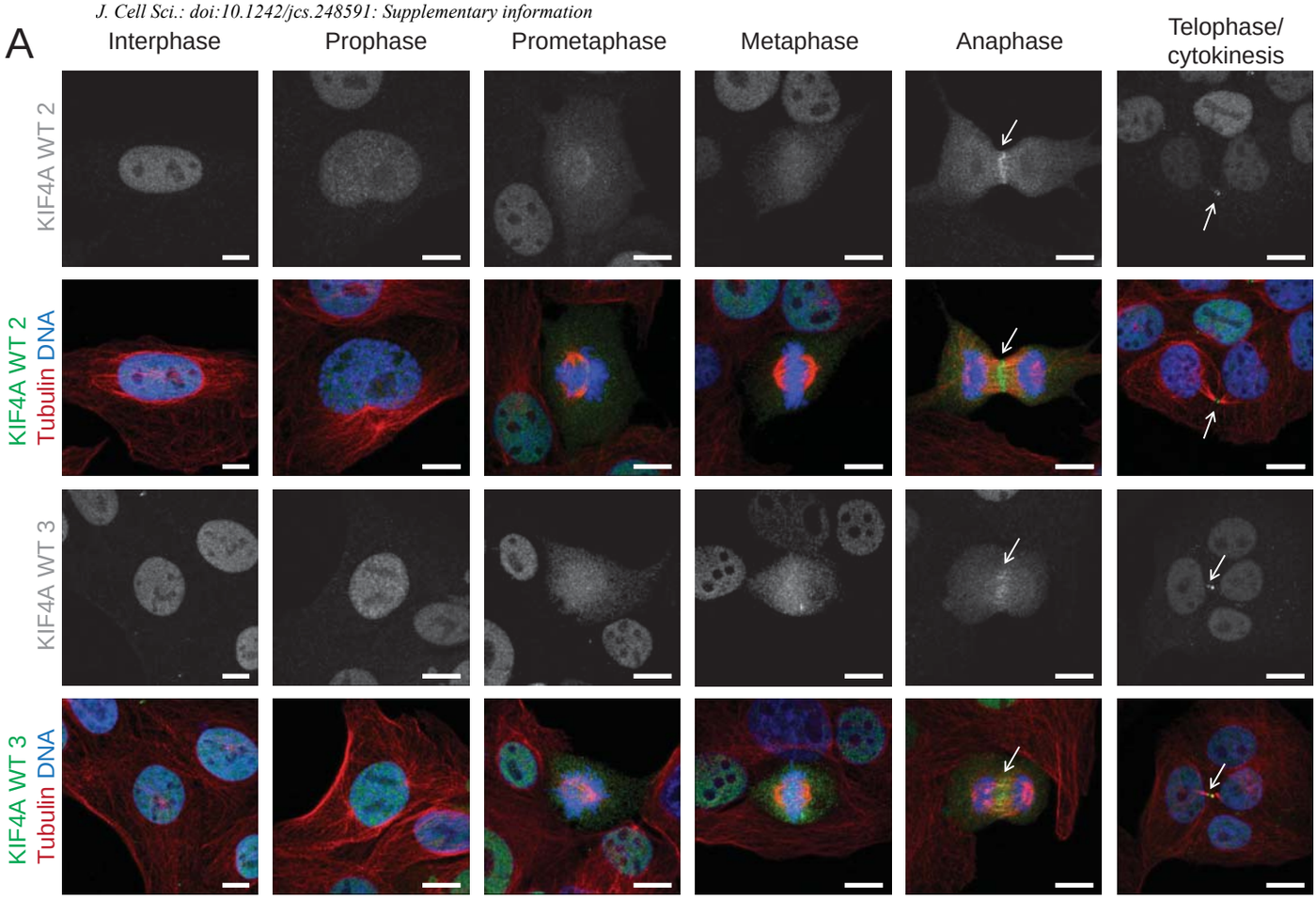

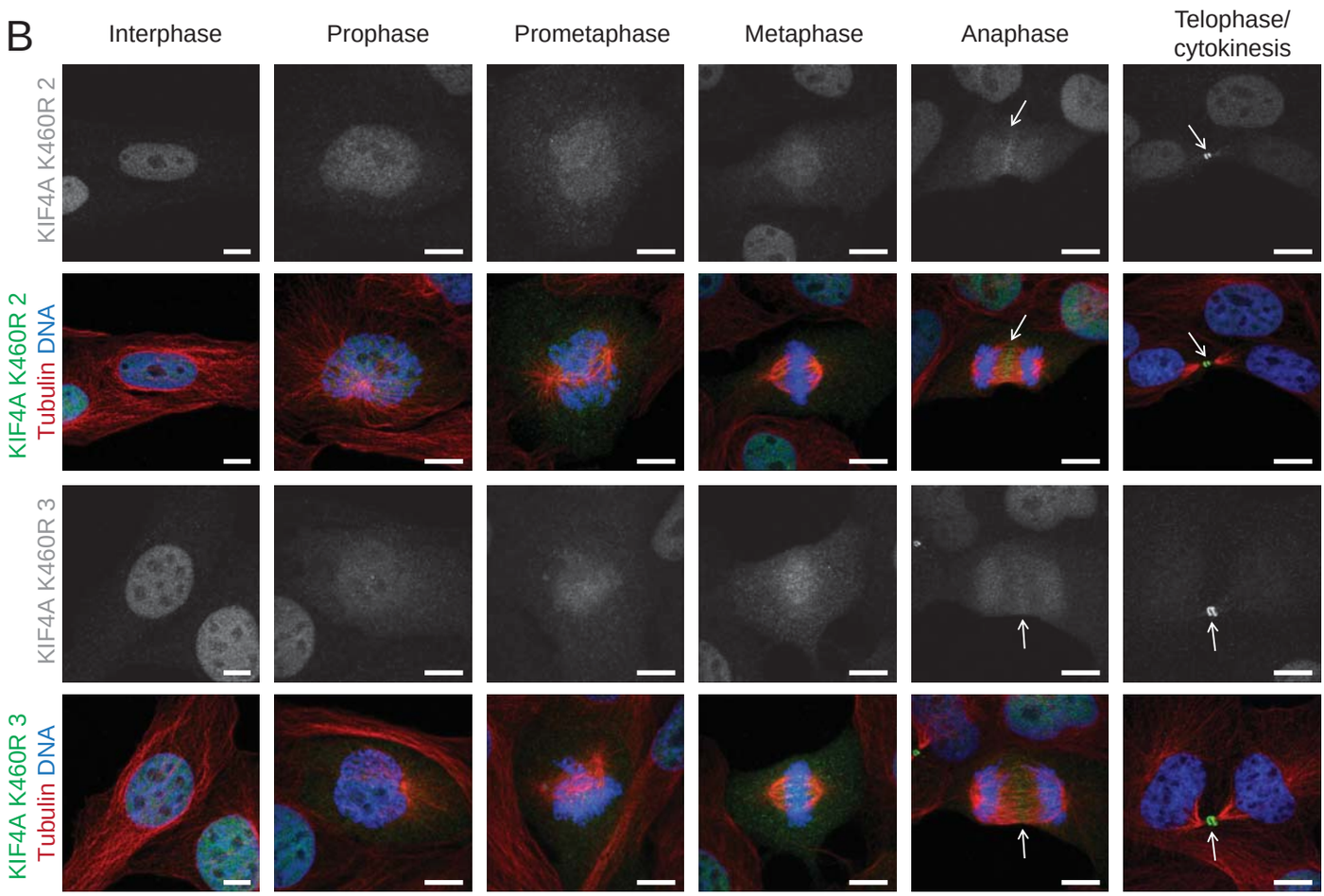

Figure S4 The localization of endogenous KIF4A during mitosis is not dependent on SUMOylation. (**A**) Two additional U2OS cell lines expressing endogenous WT KIF4A (clone 2 and 3) or (**B**) endogenous K460R KIF4A (clone 2 and 3) were grown on glass slides, fixed and stained with antibodies against KIF4A (green), tubulin (red) and Hoechst to visualize DNA (blue). Representative images were taken of cells in different stages of mitosis to visualize KIF4A localization. Scale bars correspond to 10 μm. Each experiment was performed at least three times.

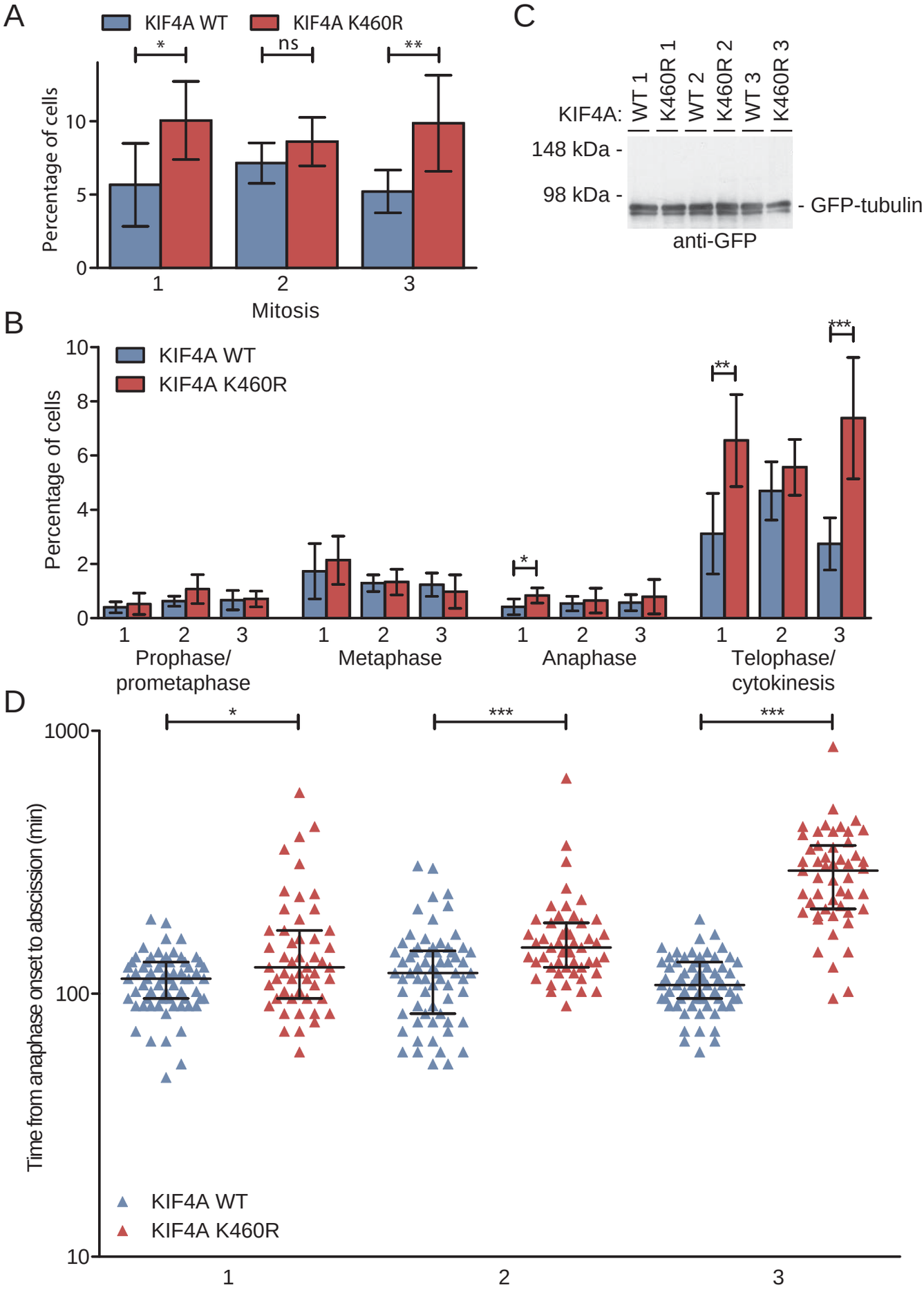

Figure S5 Increased mitotic index and delay in abscission in cells deficient for SUMOylation of endogenous KIF4A. (**A**) Three independent sets (1, 2 and 3) of KIF4A wildtype (WT) and SUMOylation deficient (K460R) clones were fixed and stained with Hoechst and antibodies directed against KIF4A and tubulin. Images were taken randomly and analyzed for the total amount of cells and the number of cells in mitosis. The mean percentage of cells in mitosis for each set of KIF4A WT and K460R clones is shown with corresponding standard deviations. P values were calculated using a two-sided Student T-test. One star represents $p < 0.05$ and two stars $p < 0.005$. ns, not significant. (**B**) The mitotic cells identified in the experiment described in Supplementary information, Figure 5A were categorized into prophase/prometaphase, metaphase, anaphase or telophase/cytokinesis. The mean percentage of cells in each phase of mitosis for each set of KIF4A WT and K460R clones is shown with corresponding standard deviations. P values were calculated using a two-sided Student T-test. One star represents $p < 0.05$, two stars $p < 0.005$ and three stars $p < 0.0005$. Each experiment was performed at least three times. (**C**) All three WT and three K460R KIF4A clones were transfected with a GFP-tubulin construct, selected using G418, subcloned and sorted by flow cytometry to obtain stable cell lines with equal GFP-tubulin expression. Cells were lysed and samples were analyzed by immunoblotting using an antibody against GFP. (**D**) Live cell imaging was used to analyze the time from anaphase onset to abscission, based on the DIC and GFP-tubulin signal for 66 cells per WT clone and 51 cells per K460R clone. Each individual cell is represented by a colored triangle, while the medians with interquartile ranges are shown in black for each set of WT and K460R clone. P values were calculated using the Mann Whitney test. One star represents $p < 0.05$ and three stars $p < 0.0005$.

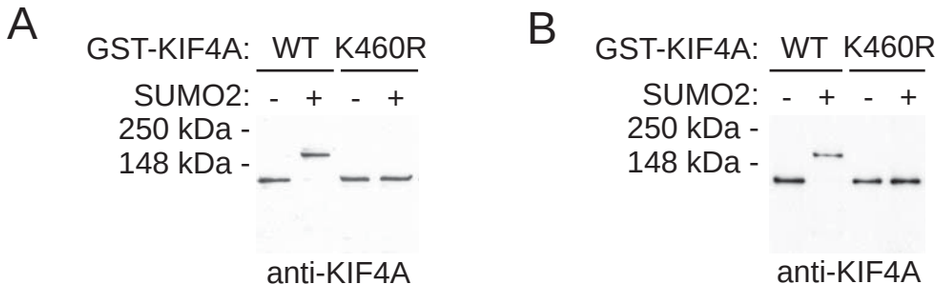

Figure S6 Confirmation of *in vitro* SUMOylation KIF4A before and after lysate incubation. (**A**) Recombinant GST-KIF4A wildtype (WT) or SUMOylation deficient mutant (K460R) were bound to beads and an *in vitro* SUMOylation assay was performed in the absence or presence of SUMO2. Aliquots of the samples were used to verify SUMOylation efficiency by immunoblotting using an antibody against KIF4A. (**B**) The samples described in Supplementary information, Figure 6A were incubated with a U2OS lysate and washed. Prior to sample preparation for mass spectrometry analysis, aliquots of the samples were saved to verify SUMOylation and protein levels by immunoblotting using an antibody against KIF4A. Each experiment was performed at least three times.

A

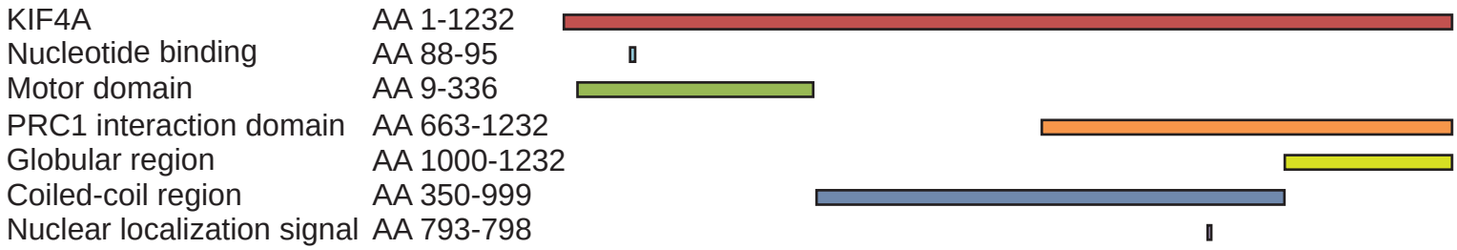

B

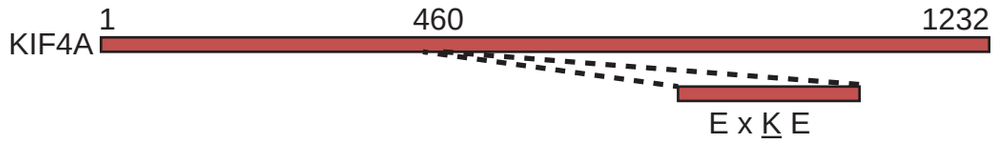

Homo sapiens	428	EKMNAKLEELRQ-------HAACKLDL-QKLVETLEDQELKENVEIICNL	469
Canis lupus familiaris	429	EKMNAKLEELRQ-------HAALKVDL-QKLVETLEDQELKENVEIIRNL	470
Bos taurus	429	EKMNAKLEELRK-------HAACKVDL-QKLVETLEDQELKENVEIIRNL	470
Mus musculus	429	EKMNAKLEELRR-------HAACKVDL-QKLVETLEDQELKENIEIICNL	470
Rattus norvegicus	429	EKMNAKLEELRQ-------HAACKVDL-QKLAETLEDQEVKENIEIICNL	470
Gallus gallus	431	EKMNAKLEQLQQ-------HAVCKLDL-QKLLETVEDEELKENVEVIRNL	472
Xenopus (Silurana) tropicalis	429	EKLASKIEELKQ-------HAACKVDL-QRLVETLEDQELKENVGVILDL	470
Drosophila melanogaster	445	DKLRSHVSELKN-------KLDQREQAQFGNENTNGDNEMRDFSLLVNRV	487
Caenorhabditis elegans	416	SRLEEDKAKLQS--------------MLTDVRNTVLNEEMLDAAEVVRSI	451
Arabidopsis thaliana	445	DKLIMIIESVRNGKSLDEIESCQNEDVGLVNKYVSKIQELEGELLHIKNL	494

C

Homo sapiens	139	SYLEIYNEEILDLLCPSRE--------------K--A-QINIREDPKEGI	171
Canis lupus familiaris	139	SYLEIYNEEILDLLCPSRE--------------K--ASQINIREDPKEGI	172
Bos taurus	139	SYLEIYNEEILDLLCPSRE--------------K--APQINIREDPKEGI	172
Mus musculus	139	SYLEIYNEEILDLLCSSRE--------------K--ATQINIREDPKEGI	172
Rattus norvegicus	139	SYLEIYNEEILDLLCSSRE--------------K--ASQINIREDPKEGI	172
Gallus gallus	139	SYLEIYNEDILDLLCSSRE--------------R--SSQISIREDPKEGI	172
Xenopus (Silurana) tropicalis	138	SYLEIYNEEILDLLYAARD--------------K--TNAISIREDPKEGI	171
Drosophila melanogaster	138	SFVELYQEQFYDLFSSKTR--------------D--KATVDIRE-VKNRI	170
Caenorhabditis elegans	136	SMFEVYGDNVYDLLRPDKV------------------KLNVHGDEKN-C	165
Arabidopsis thaliana	134	SFIEIFKEEVFDLLDSNSSALLKNDSGVQAKHTALSRAPIQIRETASGGI	183

Figure S7 KIF4A SUMOylation site and SUMO interaction motif conservation. (**A**) A cartoon depicting the localization of known domains and regions in the KIF4A protein. AA, amino acid. (**B**) Cartoon showing the localization of the SUMOylation site, containing lysine 460, in the KIF4A protein and the conservation of this region across the indicated species. (**C**) Cartoon depicting the localization of the SUMO interaction motif (SIM) in the KIF4A protein and the conservation of this region across the indicated species.

Table S1 Key of sample names. This sheet explains which sample name belongs to each exact sample measured.

Click here to Download Table S1

Table S2 A list of all peptides identified by Max Quant on the RAW Peptides sheet.

Click here to Download Table S2

Table S3 A list of all protein groups for which peptides were identified by Max Quant on the RAW ProteinGroups sheet.

Click here to Download Table S3

Table S4 A list of proteins for which their binding to KIF4A is significantly affected by SUMOylation. The line separates proteins that were identified to preferentially bind SUMOylated KIF4A (top) from the proteins that favoured binding to non-SUMOylated KIF4A (bottom).

Click here to Download Table S4